Statistical Analysis of Daily Discharge Data of the River Meuse and its Tributaries (1968 – 1998) : Assessment of Drought Sensitivity

Technical report prepared in the framework of the project:
Effect of Climate Change on the Hydrology of the River Meuse

R. Uijlenhoet, M.J.M. de Wit, P.M.M. Warmerdam and P.J.J.F. Torfs

Dutch National Research Programme on Global Air Pollution and Climate Change, Phase II (NOP-II)

Rapport 100

Sub-department Water Resources
Nieuwe Kanaal 11, 6709 PA Wageningen
The Netherlands
E-mail: www.dow.wau.nl/whh

ISSN 0926-230X

Preface

The research described in this report is part of a larger project, *Effect of Climate Change on the Hydrology of the River Meuse*, carried out in the framework of the Dutch National Research Programme on Global Air Pollution and Climate Change, Phase II (NOP-II). This larger project aims to address the problems associated with low flow situations in the Meuse basin through a combination of data analysis and modelling studies.

The majority of the research described in this report was carried out during the first few months of 2000, while the first author held an appointment as a Postdoctoral Fellow at the Water Resources Sub-department of the Department of Environmental Sciences of Wageningen University and Research Centre, The Netherlands. He is indebted to his co-authors Piet Warmerdam and Paul Torfs for providing the opportunity to become a "postdoc" in Wageningen in the first place and for their continued interest and support during the course of the project. He also enjoyed the stimulating feedback from his co-author and postdoctoral colleague Marcel de Wit during the final stages of the research project. The actual writing and editing of this report was done during the final months of 2000, while the first author had acquired an appointment as a Research Associate in the Environmental Engineering and Water Resources Program at Princeton University, USA. He is indebted to his colleagues there, Matthias Steiner and Jim Smith, for giving him the opportunity to devote precious time to finalise this report.

Since the basin of the river Meuse covers three countries (France, Belgium and The Netherlands), the streamflow data analysed in this report have different sources. The French data were kindly provided to us by the Direction Régionale de l'Environment (DIREN) de Lorraine. The streamflow data from Belgium were kindly provided by the Ministère Wallon de l'Equipement et des Transports (MET) in Namur (Mr. Dewil). Additional data and assistance during the project was provided by the Royal Meteorological Institute of Belgium in Brussels, in particular by Mr. Roulin of the Risk Analysis and Sustainable Development Section. The Dutch streamflow data were kindly provided to us by Rijkswaterstaat / RIZA (Institute for Inland Water Management and Waste Water Treatment) of the Dutch Ministry of Transport, Public Works and Water Management (Meuse at Borgharen) and by Water Authority "de Dommel" (Essche Stroom at Nemelaer and Nieuwe Leij at Goirle). All these sources are gratefully acknowledged.

The authors
Wageningen, April 2001

CONTENT

FIGURES

TABLES

TABLES Page

APPENDICES (CD included)

Figures

Matlab scripts

1. Introduction

1.1. Rationale

The rivers Rhine and Meuse fulfil important functions in the water supply of The Netherlands. Global climate change may affect the hydrological behaviour of these rivers and consequently the availability of water for a variety of purposes. The possible effects of global climate change on the discharge regime of the river Rhine system has been studied extensively during recent years. The Meuse, however, has received significantly less attention. In comparison with the river Rhine system, the Meuse system has specific characteristics and related problems:

- both the seasonal and the inter-annual variability of the hydrologic regime of the river Meuse is much more pronounced than that of the river Rhine;
- the river Meuse is likely to react much stronger to the effects of global climate change than the river Rhine, and the associated problems regarding water availability and droughts are expected to be much more pronounced.

These characteristics may be partly explained by the fact that the Meuse can be regarded as an almost purely rain-fed river, as opposed to the river Rhine, for which snowmelt in the Alpine region plays an important role. In any case, the deviating characteristics of the Meuse and the associated vulnerability of its water supply for various important socio-economic functions justify a dedicated investigation towards the possible effects of global climate change on its discharge regime.

The Meuse basin (~33000 km^2) covers parts of France, Belgium, Germany, and The Netherlands. The Meuse supplies water for domestic, industrial, and agricultural use and also fulfils navigational, ecological and recreational functions. Both prolonged wet periods and prolonged dry periods can hamper these functions. Results of experiments conducted with several general circulation models suggest that in the nearby future regional precipitation and evaporation patterns over the Meuse catchment will change significantly. In winter, increased precipitation may result in higher peak flows, while prolonged periods without sufficient precipitation combined with increased evapotranspiration rates may increase drought problems in summer.

Ideally, precipitation received by river basins is temporarily stored in natural and artificial reservoirs and released only slowly. In a mild, humid climate such as prevailing over the Meuse basin, this would ensure a continuous flow of water without extreme peak and low flow situations. This evidently requires sufficient natural and artificial storage capacity in the basin. However, as a result of increased urbanisation, land use changes, and water management measures, the buffer capacity of the Meuse basin is likely to change in such a way that river flows will be less attenuated and water is released more rapidly from the catchment. Combined with the anticipated effects of global climate change, this will increase problems in the Meuse basin during both high and low flow situations.

Most attention for the Meuse has been focused on peak flow situations in winter, when increased discharge due to increased precipitation can be expected. Low flow situations, however, when prolonged periods of little precipitation may lead to increased drought problems in the entire Meuse basin, deserve attention as well. An increase of both the

frequency and the length of dry periods can hamper many important functions of the Meuse river. The Meuse, being a typical rain-fed river, may show increased problems with low flow situations in summer and autumn, especially in regions with small infiltration rates and limited (ground)water storage capacities. In order to plan preventive measures and mitigate the impacts of drought, one needs to know which sub-catchments of the Meuse basin are most vulnerable with regard to drought.

The research described in this report is part of a larger project, *Effect of Climate Change on the Hydrology of the River Meuse*, carried out in the framework of the Dutch National Research Programme on Global Air Pollution and Climate Change, Phase II (NOP-II). This larger project aims to address the problems associated with low flow situations in the Meuse basin described above through a combination of data analysis and modelling studies. The specific part of the project to which this report is devoted, is an exploratory statistical analysis of available hydrological data for the Meuse basin, in order to identify historical dry periods and investigate the drought sensitivity of different sub-catchments. As far as possible, causes and effects of these sensitivities will be discussed as well.

1.2. Available hydrological data

Time series of mean daily discharges from several gauging stations along the Meuse and its tributaries in The Netherlands and Belgium were available for the research project described in this report through participating research institutes (see preface). These data had been used in previous research projects in which these institutes had been involved, e.g. MEUSEFLOW (Van Deursen, 1999) and SCHEME (Gellens and Roulin, 1998; Gellens *et al.*, 1998). In principle, these data could have been combined with rainfall and evaporation data available for several sites throughout the Meuse basin to study water balance characteristics.

In the framework of the project described in this report, however, a different approach was taken. Instead of analysing a combination of discharge, rainfall, and evaporation data for a relatively limited number of locations, it was decided to compile a larger dataset of discharge time series to focus the attention entirely on a detailed statistical analysis of discharges for the Meuse and its main tributaries. It appeared that such an analysis had not yet been conducted for many of the available gauging stations. As such, this study would provide both a benefit in the framework of the mentioned NOP-II project and serve the broader goal of generating regional discharge frequency information for a large part of the Meuse basin. Combining these discharge data with rainfall and evaporation data, although very interesting and useful in itself, would then be something that would fall outside the scope of this research project.

A number of additional discharge time series was obtained via collaborating institutes (see preface). In order to be able to perform a sound statistical analysis of discharge data, the time series at hand (the 'samples') should obviously have a certain minimum length. Quite arbitrarily, it was decided to take only those gauging stations into account in the current study, for which at least 10 calendar years of uninterrupted mean daily discharge data were available (i.e. data without gaps and other inconsistencies). It will be seen later that all time series except one satisfied this constraint.

This approach meant necessarily that for most gauging stations only part of the totally available data would ultimately be used for the statistical analysis described in this report. This happened to be particularly true for some of the French stations involved, for which only relatively short time series remained. Moreover, some gauging stations for which time series were available even had to be discarded altogether due to a lack of sufficiently long uninterrupted intervals. This was the case for the data from gauging stations from the Dutch Water Authority 'Roer en Overmaas', namely the Geleenbeek at Oud-Roosteren (for which only one calendar year seemed to be free of errors and inconsistencies), the Jeker at Nekum-Maastricht and the Roer at Drie Bogen (for both of which only five years of data met the mentioned criterea).

The final list of 23 gauging stations that were taken into account in this study, together with the associated periods of uninterrupted data and some other parameters of interest, is given in Table 1 and Figure 1. Note that the upstream drainage areas corresponding to these gauging stations cover more than two orders of magnitude, from a mere 94 km^2 for the Hoyoux at Modave (Belgium) to 21000 km^2 for the Meuse at Borgharen (The Netherlands).

Table 1 shows that there is only one gauging station that does not satisfy the 10 calendar year requirement, namely the Meuse at Montcy-Notre-Dame (France), for which only 8 calendar years of reliable data remained after inspection. It was nevertheless decided to take this gauging station into account, mainly because it was considered important to have a significant number of French stations involved in the analysis. The results corresponding to this station should therefore be judged accordingly. Also note that five out of the 23 gauging stations have discharge time series associated with them that cover the entire 31-year period from 1968 to 1998, corresponding to a total of 11323 mean daily discharge data.

An important point in the interpretation of the data is to note that the discharges at all gauging stations are likely to reflect some influence of human interference in the form of dams, weirs and/or sluices. The general effect of such type of interference would obviously be one of water conservation and attenuation.

A final remark concerns the fact that four gauging stations, notably all three Dutch stations, have shorter or longer periods with zero discharges associated with them. Although these periods had not previously been identified as being faulty, in most of the analyses that will be described in the sequel, they have been discarded.

Appendix 1 shows the streamflow time series corresponding to all 23 gauging stations listed in Table 1. These are the data on which all subsequent statistical analyses have been based. A visual inspection shows no signs of remaining errors or inconsistencies in the data. The characteristic pattern of flood waves, with steep rising limbs and long tails, can be discerned in all 23 discharge time series, although for each gauging station in a slightly different manner. An other objective of this research project is to try to relate the observed variability between the different gauging stations, to the geophysical characteristics that set one catchment apart from the other.

Figures 2 to 12 present the results of the analysis for all 23 stations. In this report only the results for station 1 (Amblève) are included. The results for the other stations are shown in appendices 2 to 12.

Table 1. List of gauging stations for which mean daily discharge data are analysed in this report, together with some characteristics of the corresponding catchments and time series.

#	River	Gauging station	Upstream area (km^2)	First year	Last year	# Days	# Zero runoff days
1	Amblève	Martinrive (B)	1068	1968	1998	11323	0
2	Eau Blanche	Nismes (B)	254	1969	1990	8035	0
3	Eau Noire	Couvin (B)	176	1986	1996	4018	0
4	Essche Stroom	Nemelaer (NL)	330	1973	1996	8766	2
5	Hoyoux	Modave (B)	94	1973	1987	5478	0
6	Lesse	Gendron (B)	1314	1968	1998	11323	0
7	Mehaigne	Moha (B)	343	1969	1996	10227	0
8	Meuse	Borgharen (NL)	21000	1968	1998	11323	25
9	Meuse	Chooz (F)	10120	1968	1997	10958	0
10	Meuse	Domrémy-la-Pucelle (F)	1031	1987	1996	3653	0
11	Meuse	Goncourt (F)	364	1980	1996	6210	0
12	Meuse	Montcy-Notre-Dame (F)	7724	1985	1992	2922	0
13	Meuse	Saint-Mihiel (F)	2540	1985	1996	4383	0
14	Meuse	Stenay (F)	3904	1985	1996	4383	0
15	Meuse	Vaucouleurs / Chalaines (F)	1717	1986	1996	4018	0
16	Molignée	Warnant (B)	125	1969	1996	10227	0
17	Nieuwe Leij	Goirle (NL)	115	1980	1994	5479	47
18	Ourthe	Nisramont (B)	737	1978	1996	6940	0
19	Ourthe	Tabreux (B)	1616	1968	1998	11323	0
20	Ourthe Occidentale	Ortho (B)	386	1978	1996	6940	0
21	Ourthe Orientale	Mabompré (B)	317	1978	1996	6940	0
22	Semois	Ste. Marie (B)	143	1978	1996	6940	46
23	Vesdre	Chaudfontaine (B)	677	1968	1998	11323	0

Figure 1. Location of monitoring stations

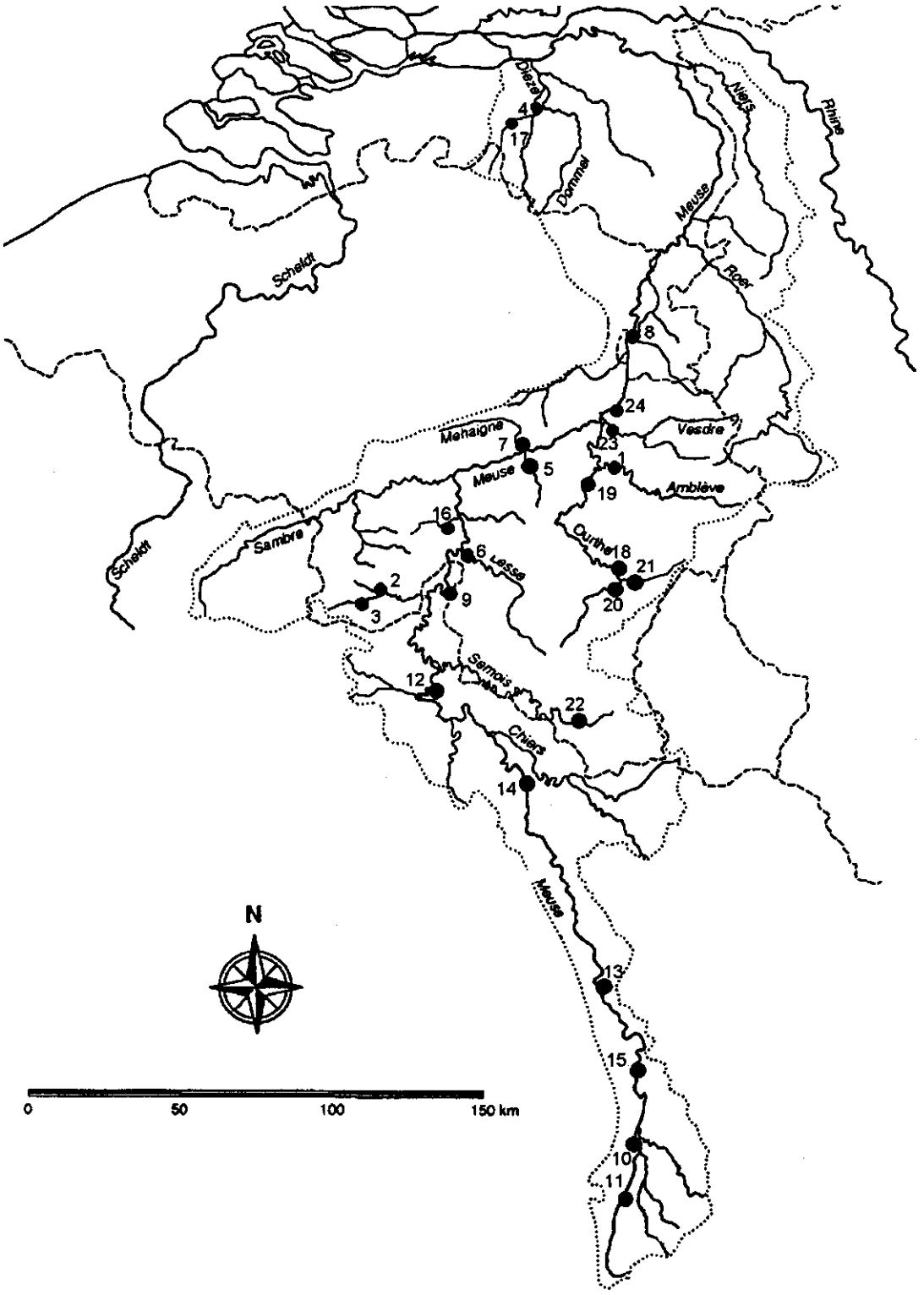

1.3. Preliminary analyses

A first thing that comes to mind when analysing discharge data for the purpose of identifying drought sensitivity (or flood sensitivity, for that matter) is to quantify the magnitudes and trends of the inter-annual and intra-annual (seasonal) variability. Figure 2 (top panel) shows the inter-annual variability of the mean daily discharge and the spread around it. There is a clear temporal dependence between total discharge volumes for subsequent years.

From a hydroclimatological perspective, droughts (and wet periods) are of particular importance when they extend over several years. To this end, the same analysis was repeated for 2-year (middle panel) and 5-year (bottom panel) moving windows. This reveals that the 1970s were basically very dry, the 1980s (starting in the late 1970s) very wet, and the 1990s (starting in the late 1980s) dry again. The same pattern seems to repeat itself for all gauging stations.

The seasonal variability of the mean daily discharge is shown in Figure 3. Apart from the expected behaviour, with low flows during summer and high flows during winter (both with their associated variability), all discharge time series seem to display a runoff peak during the second half of March. Although there exists no decisive clue as to the nature of this phenomenon, it might be due to snowmelt effects.

1.4. Overview of subsequent analyses

If the 23 discharge time series are regarded as realisations of stochastic processes, two aspects of their variability need to be distinguished: the *magnitude* of their fluctuations and the *speed* of their fluctuations. In order to assess the sensitivity of the various sub-catchments that are presented in Table 1 to droughts, both aspects require quantification. The magnitude of the daily discharge variability will be dealt with in Chapters 2 and 3 through identification of the empirical probability distributions of the mean daily discharges and their (yearly) extreme values, respectively. The speed of the daily discharge variability will be considered in Chapters 4 and 5 when dealing with the temporal dependence structure of the time series at hand: their empirical autocorrelation functions and power spectra, and their level crossing and recession properties. In Chapter 6, the results for the individual sub-catchments will be compared to each other, using the physical properties of the catchments (in this case the upstream drainage area and a rough geological characterisation) as a common denominator. Finally, Chapter 7 provides some recommendations for future research in this area.

Figure 2. Mean yearly discharge time series (top panel), 2-year aggregation (middle panel), and 5-year aggregation (bottom panel), including 10/90 (thin error bars) and 25/75 percentiles (bold error bars).

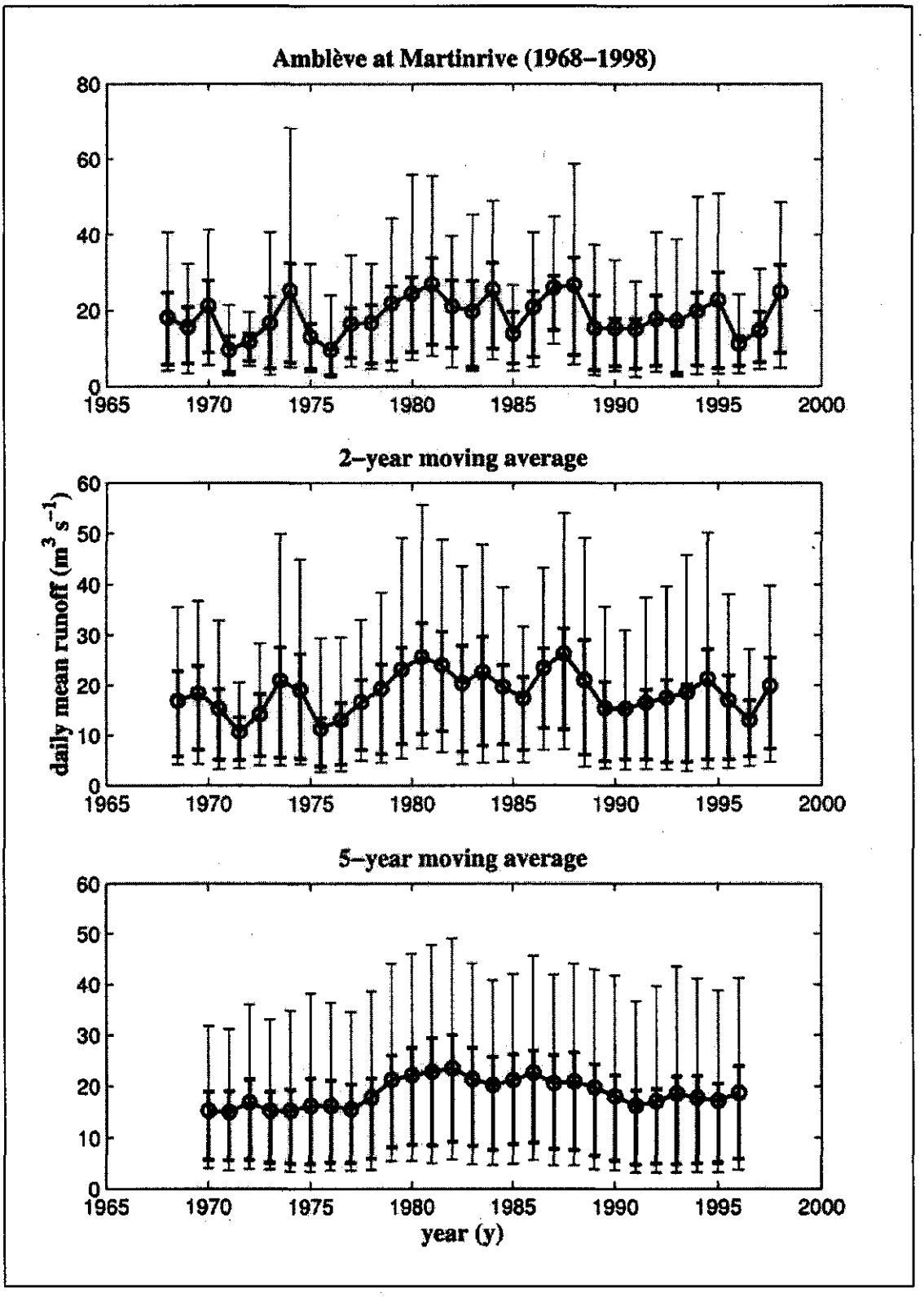

Figure 3. Mean daily discharge throughout calendar year (top panel) and 10-day aggregation (bottom panel), including 10/90 (both, thin error bars) and 25/75 percentiles (only 10-day aggregations, bold error bars).

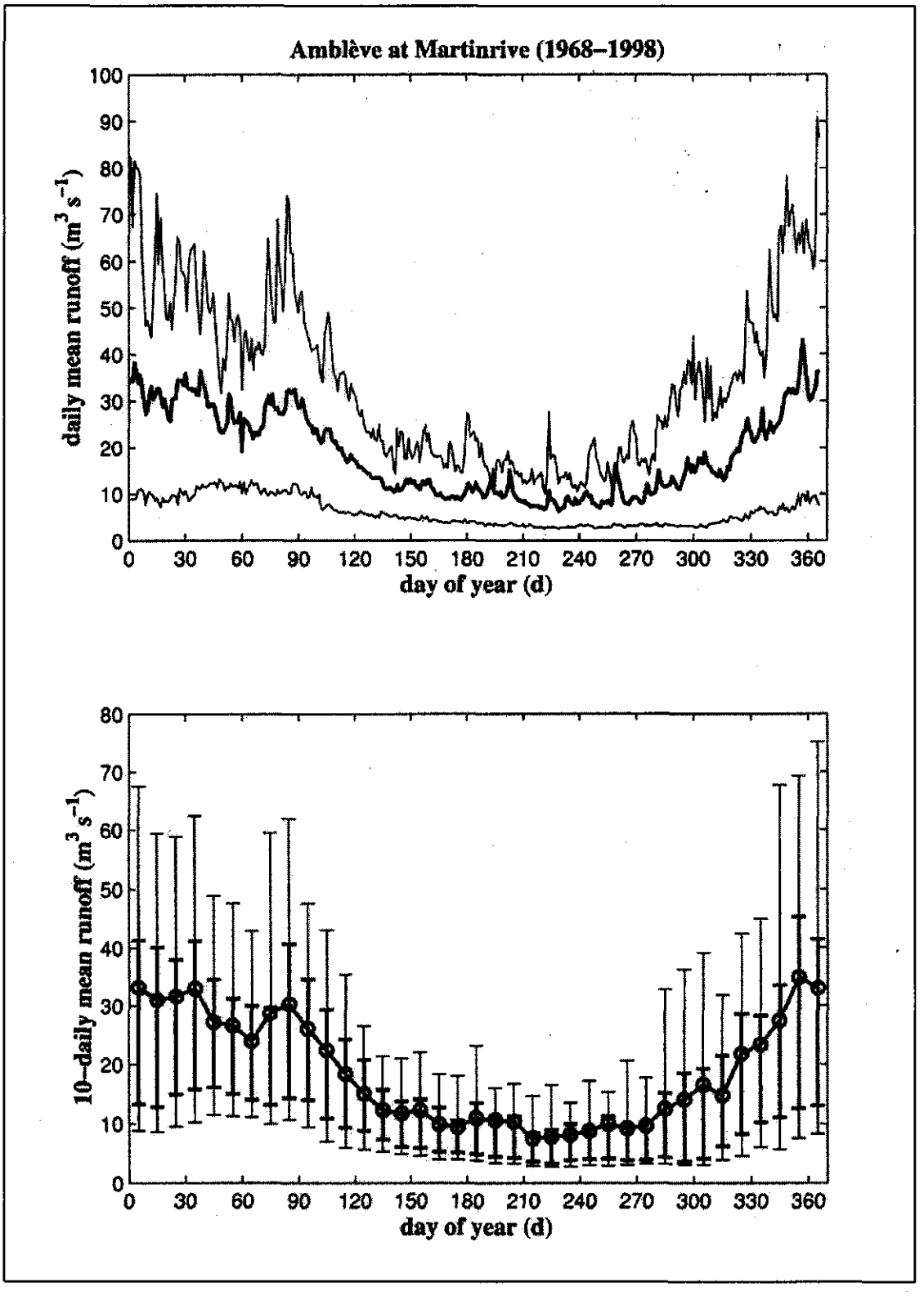

2. Frequency Analysis of Daily Discharges

Figure 4 presents three different representations of the corresponding empirical probability distribution functions. The empirical cumulative probabilities, or *plotting positions* (e.g. Haan, 1977), were determined using the formula $i/(n+1)$, where n is the total number of observations under consideration and i is the rank of the observation when all are sorted in ascending order (from 1 to n).

From the top panel plots in Figure 4 it can be seen that the marginal distributions of the discharges are strongly positively skewed for all 23 gauging stations, meaning that they have pronounced (right) tails. Straight lines on the semi-logarithmic plots in the middle panel of Figure 4 would indicate that the empirical probability distributions would have exponential tails. A visual inspection of the various plots indicates that this assertion holds rather closely for some of the catchments. Straight lines on the lognormal probability paper plots in the bottom panel of Figure 4 would indicate that the discharges would follow a lognormal (i.e. logarithmically transformed normal) distribution. This seems to hold for most of the time series, except perhaps in the extreme tails of the distributions.

Table 2 presents some numerical information regarding the empirical marginal distributions of the mean daily discharges, in the form of their statistical moments. As was the case for the upstream drainage areas (see Table 1), the mean discharges cover more than two orders of magnitude, from a mere 1.13 m^3s^{-1} for the Hoyoux at Modave (Belgium) to 227 m^3s^{-1} for the Meuse at Borgharen (The Netherlands).

The standard deviations of the discharges, a measure for the spread of the corresponding distributions, seem to follow the means rather closely. If the standard deviations are normalised through dividing them by the corresponding means, so-called *coefficients of variation* are obtained. For exponential distributions the mean equals the standard deviation (e.g. Kendall and Stuart, 1977). Therefore, they have by definition a coefficient of variation equal to unity. The empirical values are seen not to be too different from one, confirming the reasonable correspondence to the exponential distribution that follows from Figure 4.

The *coefficient of skewness*, a measure for the asymmetry of the distribution, and in particular the *coefficient of kurtosis*, a measure for its peakedness, are both significantly larger than zero. This indicates that the mean daily discharge distribution is much more asymmetric and peaked than the normal distribution, for which both these coefficients would have been zero.

To test the assertion that the empirical distribution of the mean daily discharges is closely lognormal, the calculation of the statistical moments has been repeated, but now for logarithmically transformed data (Table 3). If the data would be truly lognormally distributed, then their geometric mean would have to equal the median (e.g. Kendall and Stuart, 1977), i.e. the 50th percentile of the distribution (Table 4). This happens to be the case to a certain extent. The coefficients of variation of the logarithmically transformed data are still not that different from one, but both the coefficient of skewness and the coefficient of kurtosis are now very close to zero. The latter indicates that the logarithmically transformed data are approximately normally distributed, something that followed from Figure 4 as well.

Finally, Table 4 provides some information about the minimum and maximum mean daily discharge and three important quantiles of its empirical distribution.

3. Frequency Analysis of Annual Minima and Maxima

After having performed a frequency analysis for the actual mean daily discharges in the previous chapter, the attention is now going to be turned to a frequency analysis for the corresponding annual minima and maxima. According to extreme value theory, under certain assumptions regarding the parent distribution, the distribution of the annual minima tends to a Weibull distribution and that of the annual maxima to a Gumbel distribution (e.g. Kendall and Stuart, 1977).

Figure 5 shows plots of the annual minima series on probability paper for the lognormal and for the Weibull distribution. In addition to the annual minima series, the so-called *partial duration series* is plotted. It corresponds to the n smallest values in the sample at hand (regardless of year of occurrence), where n is the total number of years under consideration. For the lowest discharges, the annual minima series and the partial duration series will coincide. For less extreme discharges, however, the two will start to deviate, as Figure 5 clearly shows. Table 5 presents the corresponding statistics. Notwithstanding extreme value theory, the lognormal distribution seems to fit the minima at hand generally better than the Weibull distribution.

In a manner similar to that for the annual minima, Figure 6 shows plots of the annual maxima and the corresponding partial duration series. Again, the lognormal distribution provides in general at least as good a description of the data at hand as the distribution predicted by extreme value theory, the Gumbel distribution. Table 6 confirms this observation. The two series again coincide for the most extreme values and start to deviate for less extreme values. Of course, the deviation is now the inverse of what was the case for the annual minima series.

Figure 4. Three different representations of cumulative distribution of daily discharges: direct (top panel), on exponential probability paper (middle panel), and on lognormal probability paper (bottom panel). Dashed line indicates mean daily discharge.

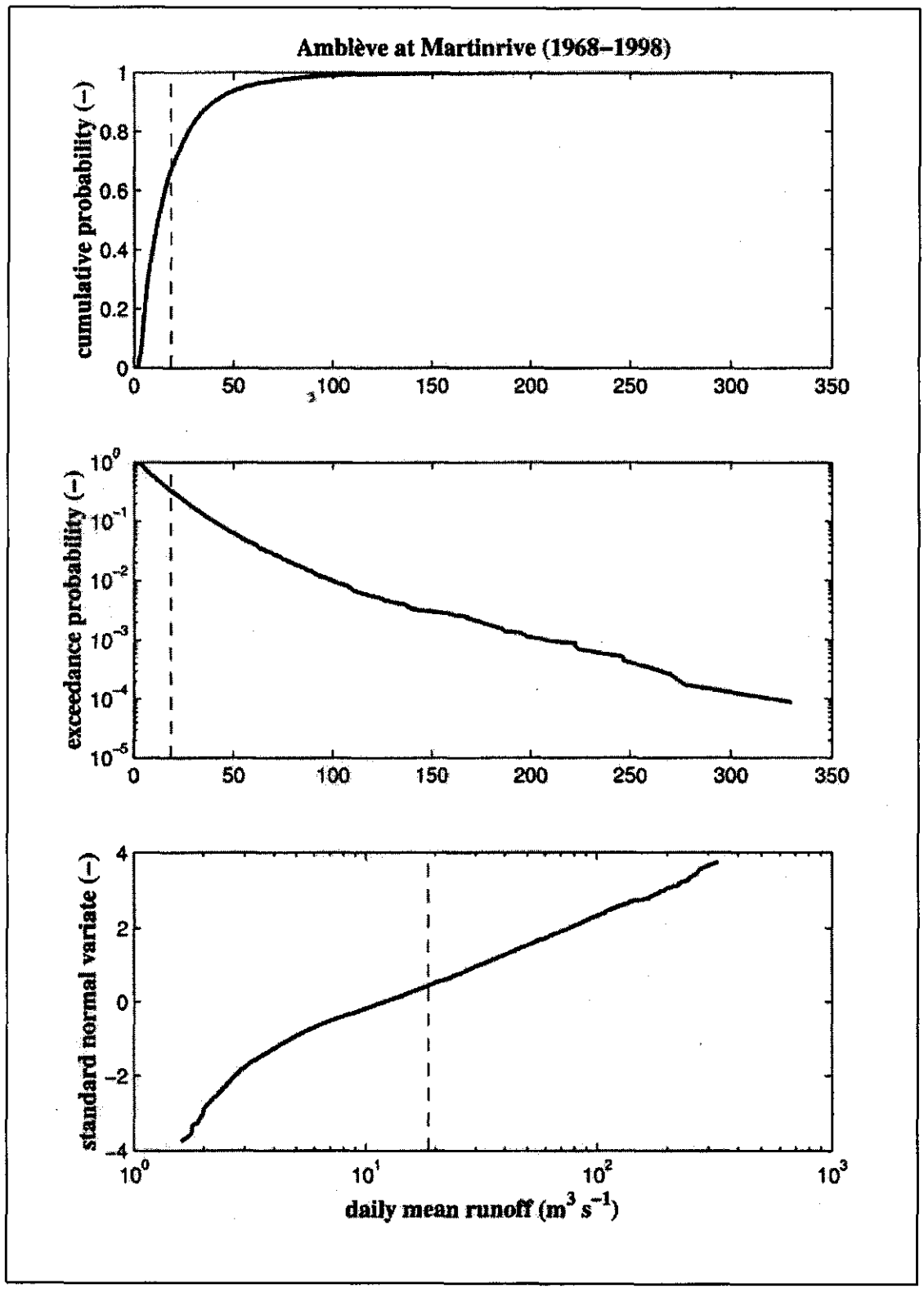

Table 2. Statistical moments of the empirical distributions of the analysed mean daily discharge time series.

#	Mean daily discharge (m^3s^{-1})	Standard deviation (m^3s^{-1})	Coefficient of variation (-)	Coefficient of skewness (-)	Coefficient of kurtosis (-)
1	18.6	20.7	1.11	3.91	27.3
2	3.12	4.49	1.44	3.07	13.1
3	3.08	5.05	1.64	5.60	56.9
4	3.08	2.84	0.922	2.54	8.68
5	1.13	0.593	0.523	1.35	2.99
6	17.4	21.8	1.25	3.91	29.7
7	2.45	2.35	0.958	3.74	21.5
8	227	268	1.18	2.67	11.4
9	147	151	1.03	2.50	9.50
10	11.1	18.1	1.64	3.35	13.6
11	4.28	7.84	1.83	3.50	15.5
12	100	94.7	0.947	2.10	5.77
13	29.7	41.2	1.39	3.12	13.3
14	46.7	52.1	1.12	2.81	10.5
15	21.4	33.3	1.56	3.22	13.2
16	1.38	1.12	0.811	4.54	43.9
17	0.923	1.23	1.33	3.04	11.8
18	13.0	16.0	1.23	3.61	22.0
19	22.2	27.0	1.22	3.66	22.7
20	6.88	8.06	1.17	3.50	21.4
21	5.34	6.53	1.22	3.97	30.1
22	2.44	3.41	1.40	3.65	16.9
23	10.3	11.5	1.12	4.67	34.7

Table 3. Statistical moments of the empirical distributions of the logarithmically transformed mean daily discharge time series.

#	Geometric mean daily discharge (m^3s^{-1})	Logarithmic coefficient of variation (-)	Logarithmic coefficient of skewness (-)	Logarithmic coefficient of kurtosis (-)
1	12.3	1.09	0.259	-0.490
2	1.47	1.87	0.287	-0.804
3	1.48	1.75	0.312	-0.503
4	2.25	0.914	0.178	-0.047
5	0.996	0.546	-0.049	-0.453
6	9.99	1.45	0.089	-0.597
7	1.86	0.797	0.528	0.108
8	115	2.20	-0.694	0.660
9	97.6	1.11	0.230	-0.645
10	4.62	2.11	0.349	-0.638
11	1.23	3.89	0.069	-0.664
12	68.5	1.08	-0.001	-0.182
13	14.8	1.77	0.197	-0.772
14	29.7	1.18	0.267	-0.650
15	9.78	1.79	0.539	-0.625
16	1.14	0.626	0.772	0.579
17	0.453	2.06	-0.328	-0.178
18	7.48	1.49	-0.025	-0.553
19	13.0	1.42	-0.002	-0.463
20	4.12	1.38	0.048	-0.728
21	3.13	1.42	0.054	-0.656
22	1.44	1.21	0.551	0.349
23	7.43	0.862	0.639	0.467

Table 4. Extremes and quantiles of the empirical distributions of the analysed mean daily discharge time series.

#	Minimum discharge (m^3s^{-1})	10^{th} percentile (m^3s^{-1})	Median discharge (m^3s^{-1})	90^{th} percentile (m^3s^{-1})	Maximum discharge (m^3s^{-1})
1	1.60	3.96	12.0	40.0	330
2	0.094	0.307	1.35	8.54	51.1
3	0.101	0.329	1.34	7.90	95.1
4	0.010	0.840	2.22	6.25	28.4
5	0.291	0.498	1.01	1.96	5.14
6	0.644	2.39	9.84	40.9	413
7	0.402	0.782	1.74	4.74	28.5
8	1.00	19.0	135	570	2959
9	10.2	32.4	92.5	342	1527
10	0.385	0.917	3.93	28.8	151
11	0.012	0.142	1.14	12.8	75.3
12	0.911	21.9	67.5	224	750
13	1.02	3.11	14.2	75.5	416
14	3.50	8.53	28.5	101	468
15	0.803	2.52	7.90	57.0	308
16	0.325	0.599	1.02	2.51	24.2
17	0.010	0.080	0.530	2.17	10.9
18	0.358	1.77	7.87	30.4	198
19	0.644	3.35	13.1	51.0	370
20	0.460	0.983	4.33	15.7	106
21	0.322	0.740	3.26	12.3	111
22	0.018	0.478	1.27	5.64	36.2
23	0.581	3.21	6.70	20.5	166

Figure 5. Plots of annual minimum series (circles) and partial duration series (plusses) of (non-zero) daily discharges on lognormal (top panel) and Weibull (bottom panel) probability paper. Dashed lines indicate linear regression of logarithm of minimum daily mean discharge (dependent variable) versus standard normal and standard Weibull variates (independent variables).

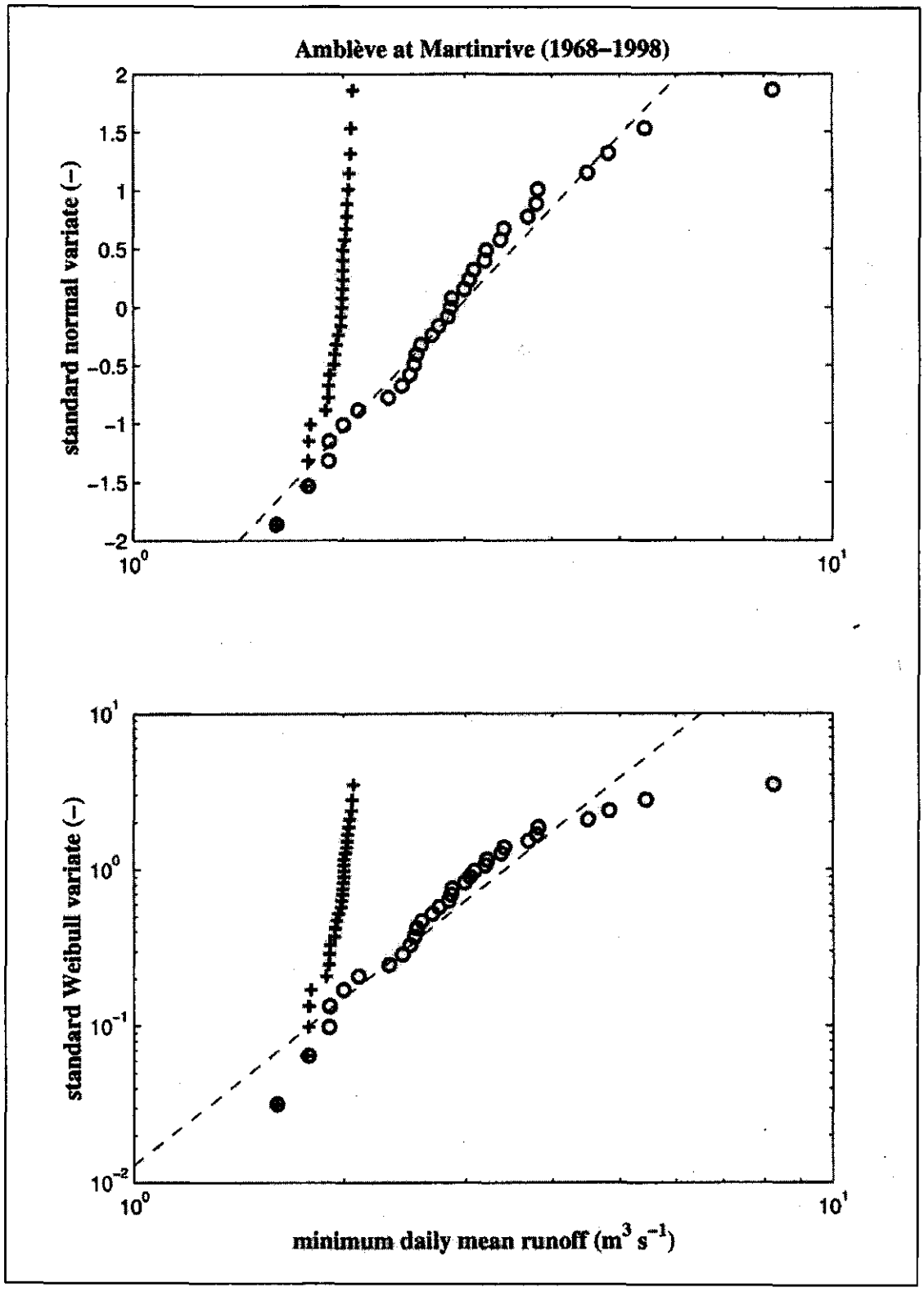

Figure 6. Plots of annual maximum series (circles) and partial duration series (plusses) of daily discharges on lognormal (top panel) and Gumbel (bottom panel) probability paper. Dashed lines indicate linear regression of (logarithm of) maximum daily mean discharge (dependent variable) versus standard normal and standard Gumbel variates (independent variables)

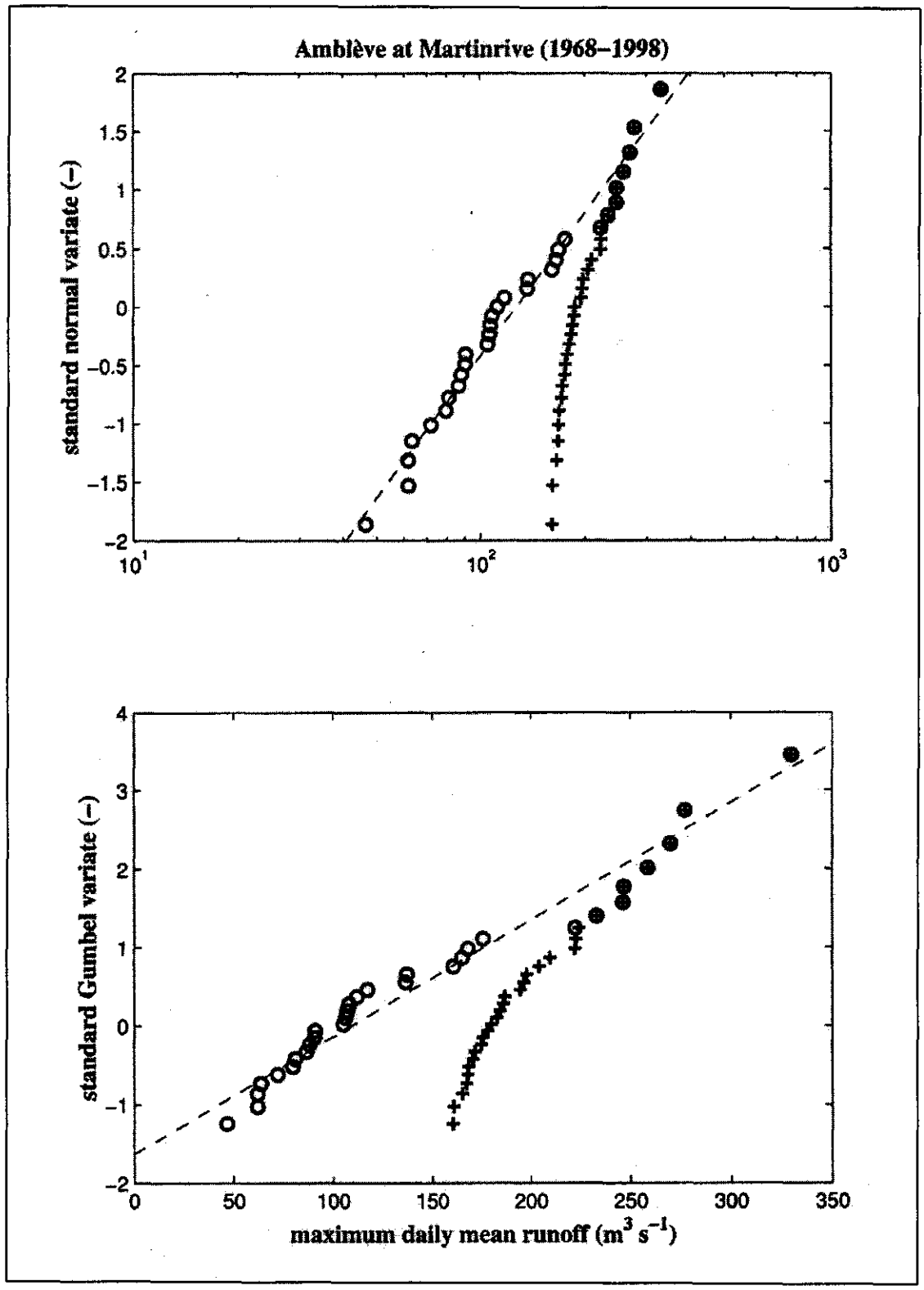

Table 5. Statistical properties of the annual minima of the analysed time series.

#	Mean annual minimum discharge (m^3s^{-1})	Standard deviation (m^3s^{-1})	Coefficient of determination of linear regression (-)	
			Lognormal paper	Weibull paper
1	3.12	1.29	0.943	0.863
2	0.268	0.093	0.928	0.952
3	0.266	0.172	0.888	0.819
4	0.581	0.266	0.572	0.681
5	0.611	0.247	0.977	0.953
6	2.08	1.15	0.930	0.852
7	0.763	0.292	0.957	0.888
8	9.87	14.4	0.911	0.871
9	26.0	9.89	0.983	0.962
10	0.748	0.382	0.924	0.863
11	0.068	0.064	0.954	0.908
12	10.0	4.69	0.650	0.753
13	2.56	1.52	0.979	0.924
14	7.01	3.09	0.976	0.933
15	1.91	0.604	0.896	0.955
16	0.576	0.131	0.974	0.980
17	0.037	0.033	0.912	0.837
18	1.14	0.833	0.942	0.862
19	2.61	1.47	0.982	0.959
20	0.839	0.552	0.815	0.685
21	0.624	0.374	0.893	0.777
22	0.335	0.186	0.711	0.780
23	2.68	0.959	0.865	0.948

Table 6. Statistical properties of the annual maxima of the analysed time series.

#	Mean annual maximum discharge (m^3s^{-1})	Standard deviation (m^3s^{-1})	Coefficient of determination of linear regression (-)	
			Lognormal paper	Gumbel paper
1	145	77.7	0.974	0.960
2	28.9	8.66	0.983	0.989
3	40.0	21.2	0.930	0.857
4	16.3	5.45	0.877	0.899
5	3.23	1.30	0.878	0.893
6	140	69.7	0.940	0.863
7	16.1	6.40	0.966	0.964
8	1417	577	0.992	0.985
9	749	289	0.972	0.958
10	115	25.9	0.937	0.922
11	53.6	14.2	0.937	0.920
12	446	157	0.957	0.960
13	256	103	0.912	0.915
14	296	116	0.929	0.921
15	218	58.2	0.878	0.874
16	7.87	4.90	0.955	0.887
17	7.64	2.32	0.933	0.923
18	108	48.7	0.973	0.962
19	174	79.1	0.984	0.979
20	54.3	24.5	0.974	0.975
21	47.4	26.2	0.983	0.973
22	23.6	5.52	0.892	0.923
23	90.4	43.0	0.943	0.945

4. Correlation and Spectral Analysis of Daily Discharges

As was mentioned in Section 1.4, the characterisation of a fluctuating signal concerns not only the magnitude of the fluctuations, but their speed as well. In this chapter and the following, the main concern will be the latter. Figure 7 shows the empirical autocorrelation functions and (two-sided) power spectral density functions corresponding to the discharge time series. An appealing property of the two-sided spectrum is that it has unit area (VanMarcke, 1983). It can therefore be simply interpreted as the normalised (probability) distribution of the variance (i.e. the power) over the different frequencies.

As was clear from Figure 3, the discharge time series at hand possess both a random and a deterministic component. The latter is mainly determined by the intra-annual (i.e. *seasonal*) periodicity of the mean and the variance of the mean daily discharge. Figure 2 shows that the deterministic component of the inter-annual variability (which could be termed *climatological* variability) is very small, particularly at the time scales that are of concern here (order of months). A correction for seasonal periodicity was applied to the data by subtracting the mean for each day and dividing by the standard deviation for each day (as obtained from Figure 3). The autocorrelation functions and power spectra were both calculated for the raw and for the corrected data. Figure 7 shows clearly that the effect of correcting is to eliminate the influence of the seasonal periodicity in both the empirical autocorrelation functions and the power spectra, as would be expected.

The 99% confidence limits on the autocorrelation function were calculated from theoretical expressions for the mean and variance of the sampling distribution of the autocorrelation coefficient given that the true autocorrelation coefficient is zero (e.g. Kendall and Stuart, 1977). It was assumed that the sampling distribution was normal.

Table 7 gives some numerical properties of the empirical autocorrelation functions and spectra. The decorrelation time is defined as the time where the autocorrelation for the first time drops below the upper 99% confidence line (i.e. for the first time is not significantly different from zero), or 366 days, whichever is smaller. The scale of fluctuation is defined as twice the integral under the autocorrelation function between zero and the decorrelation time (VanMarcke, 1983). Theoretically, the two-sided power spectral density at zero frequency corresponds to the scale of fluctuation (VanMarcke, 1983). However, as the lower panel of Figure 7 shows, there may be small deviations due to the non-stationarity and discreteness of the data and the fact that the decorrelation time is finite. These deviations provide some idea as to how accurate the scale of fluctuation may be estimated. This will be important when comparing the scale of fluctuation with other estimates of characteristic time scales of the discharge time series.

Figure 7. Empirical autocorrelation function (direct, top panel, and semi-logarithmically, middle panel) and two-sided spectral density function (bottom panel) of daily discharges, with (bold lines) and without (thin lines) correction for seasonal periodicity in mean and standard deviation. In top two panels, dashed horizontal lines indicate regions where autocorrelation significantly (with 99% confidence) departs from zero and dash-dotted vertical lines indicate scale of fluctuation of periodicity-corrected data. In bottom panel, crosses indicate spectral densities at zero frequency, circle indicates scale of fluctuation of periodicity-corrected data, and vertical lines indicate frequencies of once per week (solid), once per month (dashed), and once per year (dash-dotted).

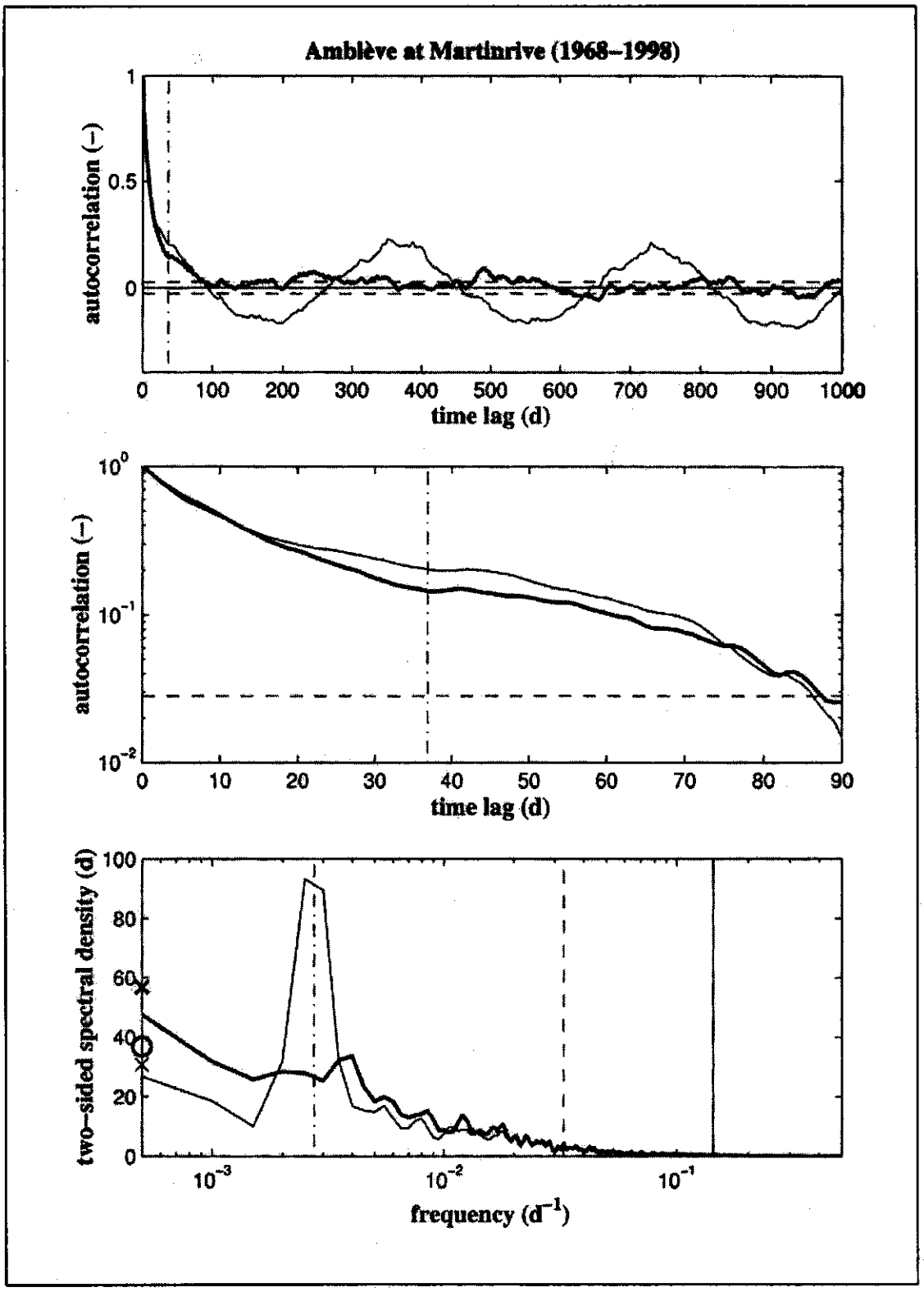

Table 7. Some properties of the empirical autocorrelation functions of the analysed time series, with and without correction for seasonal periodicity in mean and standard deviation.

#	First order autocorrelation coefficient (-)		Decorrelation time (d)		Scale of fluctuation (d)	
	Not corrected	Corrected	Not corrected	Corrected	Not corrected	Corrected
1	0.909	0.915	87	88	40.8	36.8
2	0.851	0.860	90	97	33.1	34.2
3	0.796	0.875	88	133	31.9	49.9
4	0.927	0.904	104	295	64.3	102
5	0.959	0.973	366	366	281	430
6	0.920	0.924	91	119	45.3	43.7
7	0.912	0.902	124	366	56.8	149
8	0.967	0.941	94	198	58.8	64.3
9	0.981	0.964	95	366	66.5	111
10	0.893	0.915	76	102	35.0	49.1
11	0.831	0.856	82	85	30.9	30.4
12	0.983	0.951	83	363	55.9	143
13	0.955	0.964	83	98	48.3	53.0
14	0.980	0.979	87	356	60.2	129
15	0.904	0.923	82	81	38.2	41.0
16	0.909	0.934	115	366	61.2	148
17	0.892	0.892	96	288	46.8	78.7
18	0.939	0.934	81	88	45.8	47.0
19	0.939	0.938	89	118	45.5	42.0
20	0.940	0.938	80	82	46.7	46.6
21	0.918	0.933	86	123	44.2	48.1
22	0.823	0.815	75	74	26.9	24.6
23	0.830	0.870	95	194	31.6	46.0

5. Level Crossings and Recession Analysis

Another way to look at the aspect of the speed of discharge fluctuations, apart from analysing its correlation structure, is to calculate the number of times a particular pre-defined discharge level is crossed in a particular time interval and analyse the empirical probability distributions of the lengths of the excursions above and below that particular level and the correlation structure of those excursions (e.g. Sen, 1980). Figure 8 (top panel) provides the level crossing analyses. To allow easy comparison between the results for the different stations, the discharge levels are expressed in terms of cumulative probabilities (corresponding to Figure 4, top panel). It is interesting to see that some stations have the majority of their crossings at the centre of the probability scale, yielding a more or less symmetrical "crossing spectrum", whereas others have their modes at the low or high probability ends, giving (positively or negatively) skewed crossing spectra. It is not immediately evident how the shapes of these crossing spectra should be interpreted in terms of the physical characteristics of the corresponding sub-catchments.

Besides the number of crossings in a particular time interval, the distributions of the lengths of excursions below ("dry spells") and above ("wet spells") particular discharge levels are of interest here. This type of information is provided by the middle and bottom panels of Figure 8, and by Figs. 9 and 10 (which provide in essence the same analysis as Figure 4 provided for the discharges themselves). From these figures it follows that both the dry spells and the wet spells are characterised by very broad, positively skewed empirical distributions. The distributions of the dry spells (at least at a cumulative probability level of 10%) can be reasonably well parameterised by both the exponential and the lognormal distribution. For the wet spells, the empirical distributions seem to be more erratic. However, they are of less relevance here.

Again, it is not only the magnitude of the fluctuations of the dry and wet spells that is of interest here, but the speed of their fluctuations as well. Figure 11 provides information about the first order autocorrelation coefficients between subsequent dry spells, subsequent wet spells and subsequent dry and wet spells. It follows from this figure that neither of those combinations exhibit statistically significant correlations. This suggests that subsequent dry and wet spells could be independent, a finding that could prove very valuable from a simulation perspective.

Finally, the algorithm that was developed to detect the dry spells has been used as a starting point for an automated procedure to calculate recession coefficients, based on exponentially decaying flood peak tails (consistent with the linear reservoir model). The criteria used to calculate the recession coefficients were:

- the length of a recession period, defined as the length of the interval between the beginning of a dry spell and the day with the minimum discharge during the dry spell, has to be at least 60 days;

- the correlation coefficient between the logarithm of the discharges during the recession period and the corresponding day numbers has to be negative;

- the coefficient of determination of a linear regression between the logarithm of the discharges during the recession period and the corresponding day numbers (i.e. the square of the correlation coefficient) has to be at least 0.7.

Figure 12 provides a graphic representation of the results of this recession analysis, including uncertainties in the estimated recession coefficients and in the estimated coefficients of determination. The procedure needs additional fine-tuning, but seems to be an interesting and efficient approach to calculating recession coefficients. Table 8 summarises the results numerically.

Figure 8. Mean annual number of crossings (top panel), mean (solid line) and standard deviation (dashed line) of lengths of dry spells (middle panel), and mean (solid line) and standard deviation (dashed line) of lengths of wet spells (bottom panel) associated with 50 quantiles of daily discharge (linearly spaced between 0.001 and 0.999). In bottom two panels, error bars indicate values of minimum and maximum length of dry and wet spells at given quantile.

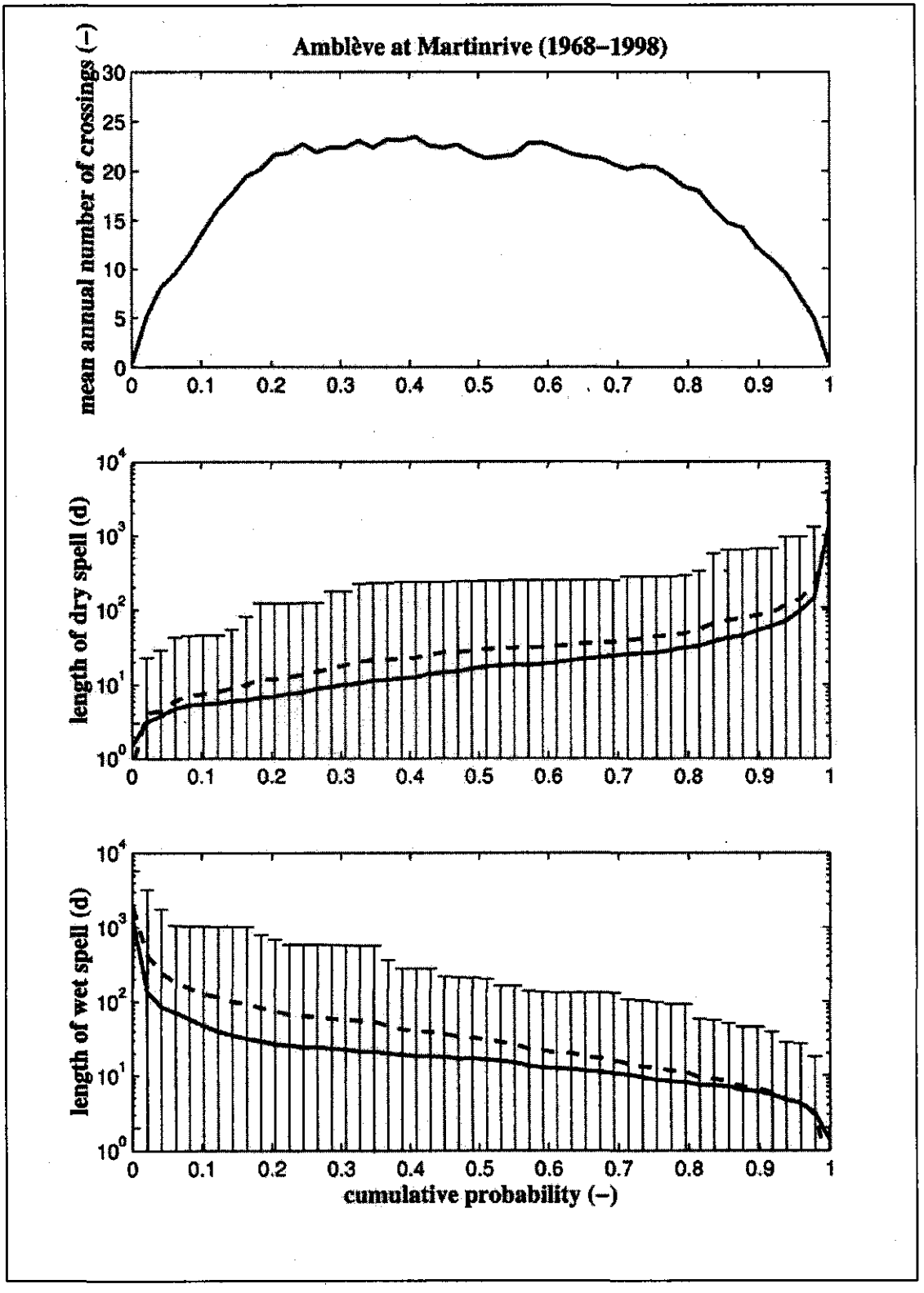

Figure 9. Three different representations of cumulative distribution of lengths of dry spells associated with 10th percentile of daily discharges: direct (top panel), on exponential probability paper (middle panel), and on lognormal probability paper (bottom panel). Dashed lines indicate mean length of dry spell at given quantile.

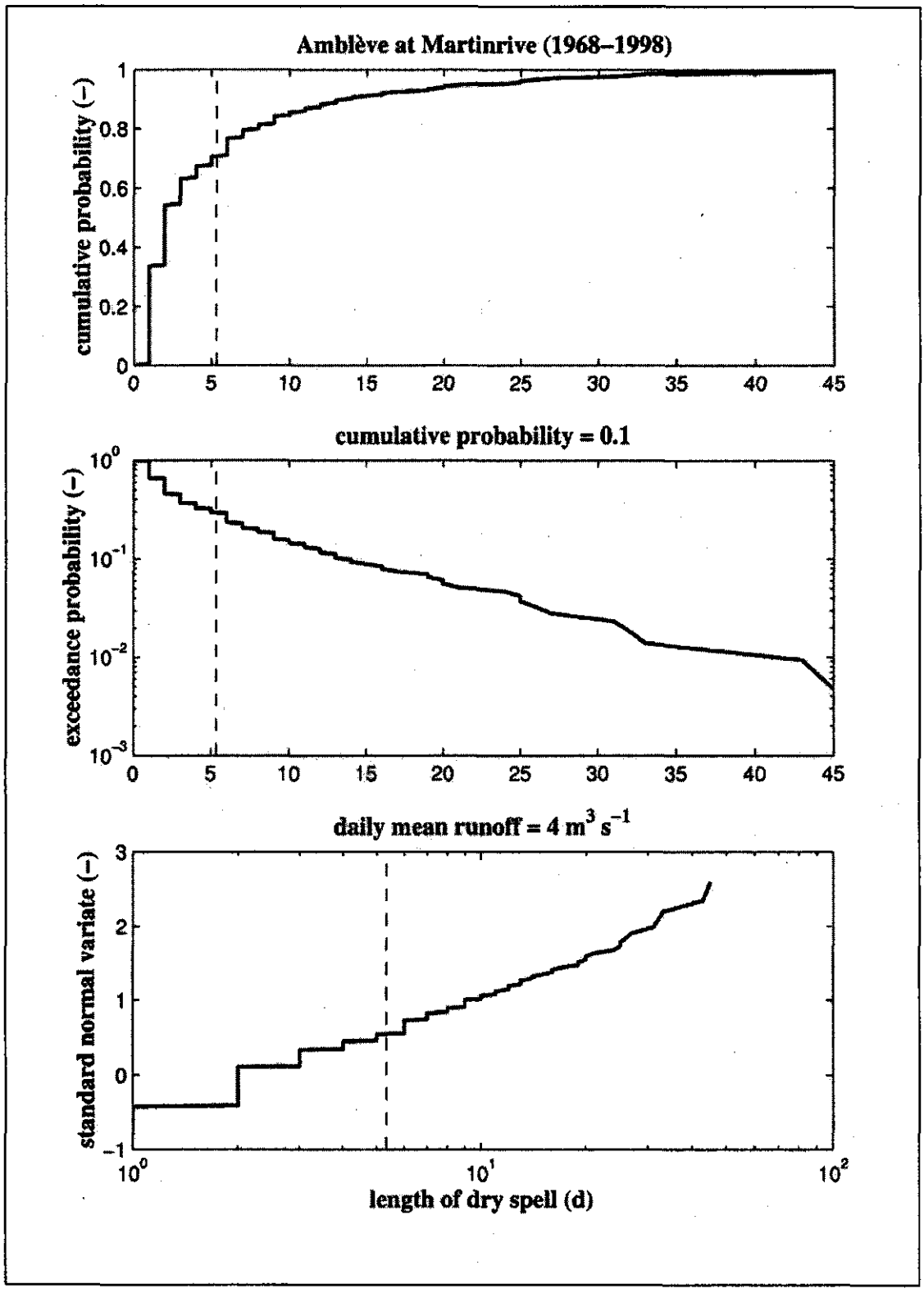

Figure 10. Three different representations of cumulative distribution of lengths of wet spells associated with 10th percentile of daily discharges: direct (top panel), on exponential probability paper (middle panel), and on lognormal probability paper (bottom panel). Dashed lines indicate mean length of wet spell at given quantile.

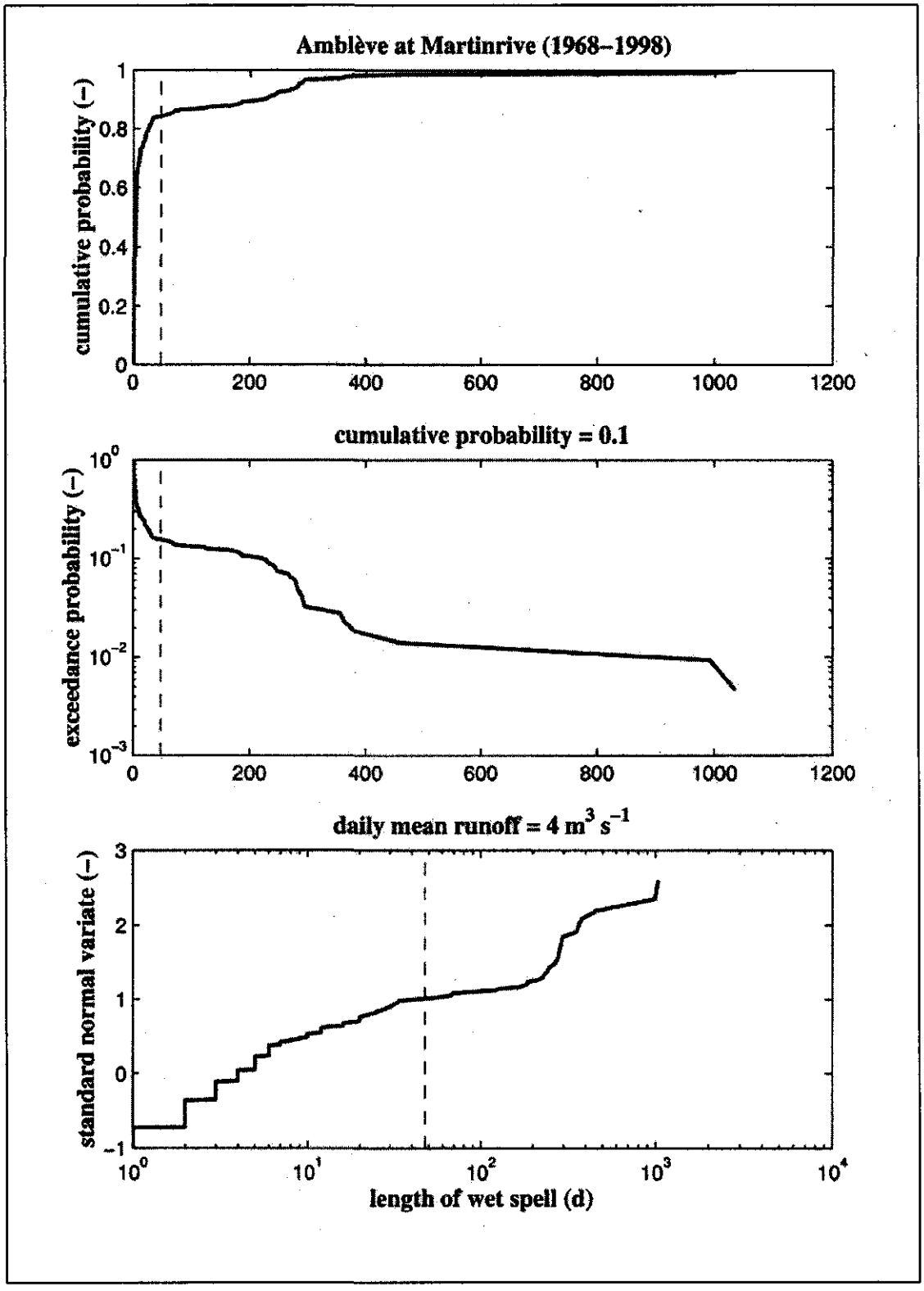

Figure 11. First order autocorrelation coefficients of subsequent dry spells (top panel), wet spells (middle panel) and dry and wet spells (bottom panel) associated with given quantiles of daily discharges for 23 gauging stations in Meuse catchment. Dashed lines indicate regions where autocorrelation significantly (with 99% confidence) departs from zero.

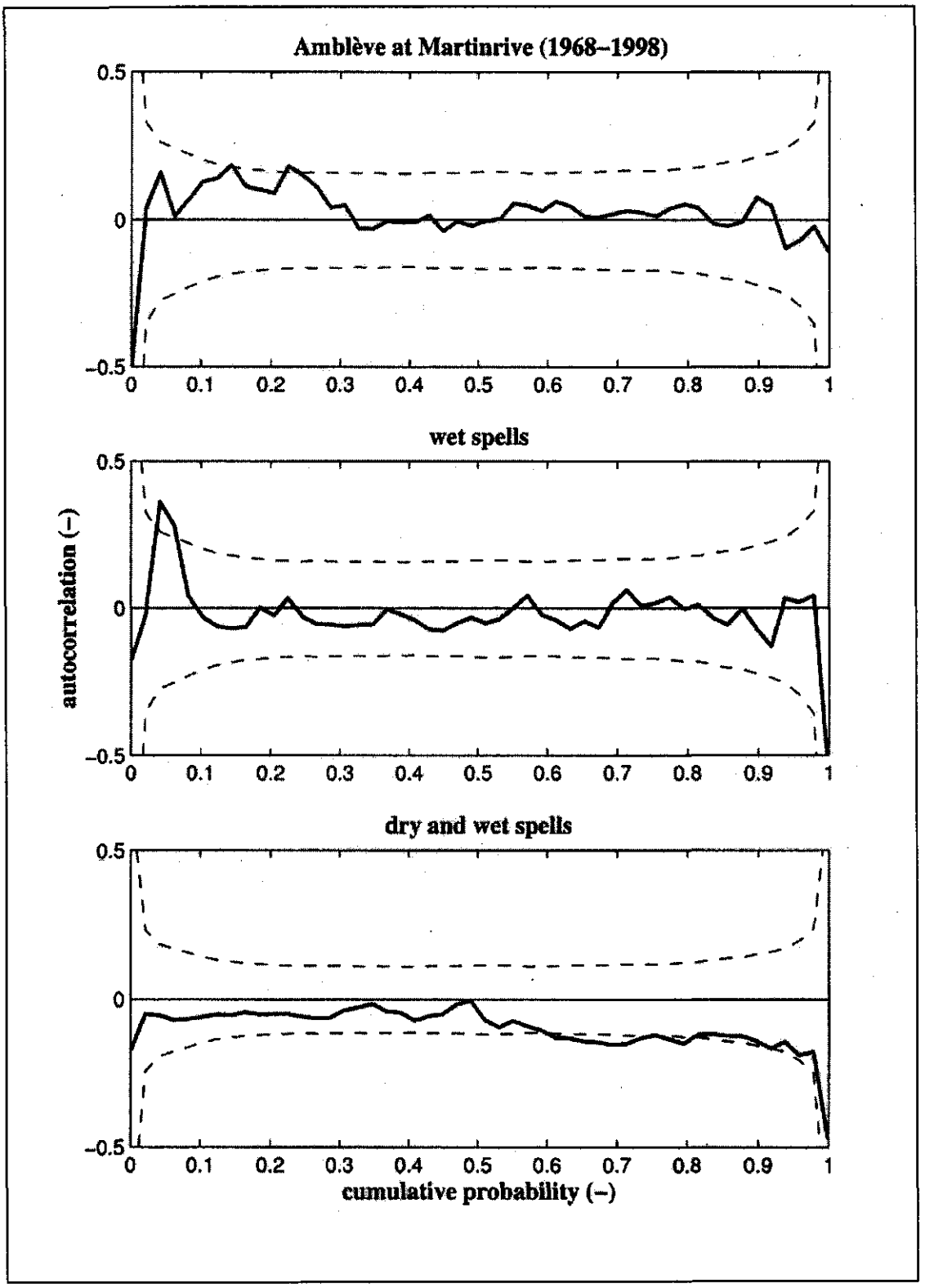

Figure 12. Recession coefficients (top panel, circles / bold solid line) and corresponding coefficients of determination (bottom panel, circles / bold solid line) associated with given quantiles of daily discharges. Error bars indicate minimum and maximum values at given quantile and bold dashed lines indicate mean values over all quantiles. Thin dashed line in top panel indicates scale of fluctuation of periodicity-corrected data.

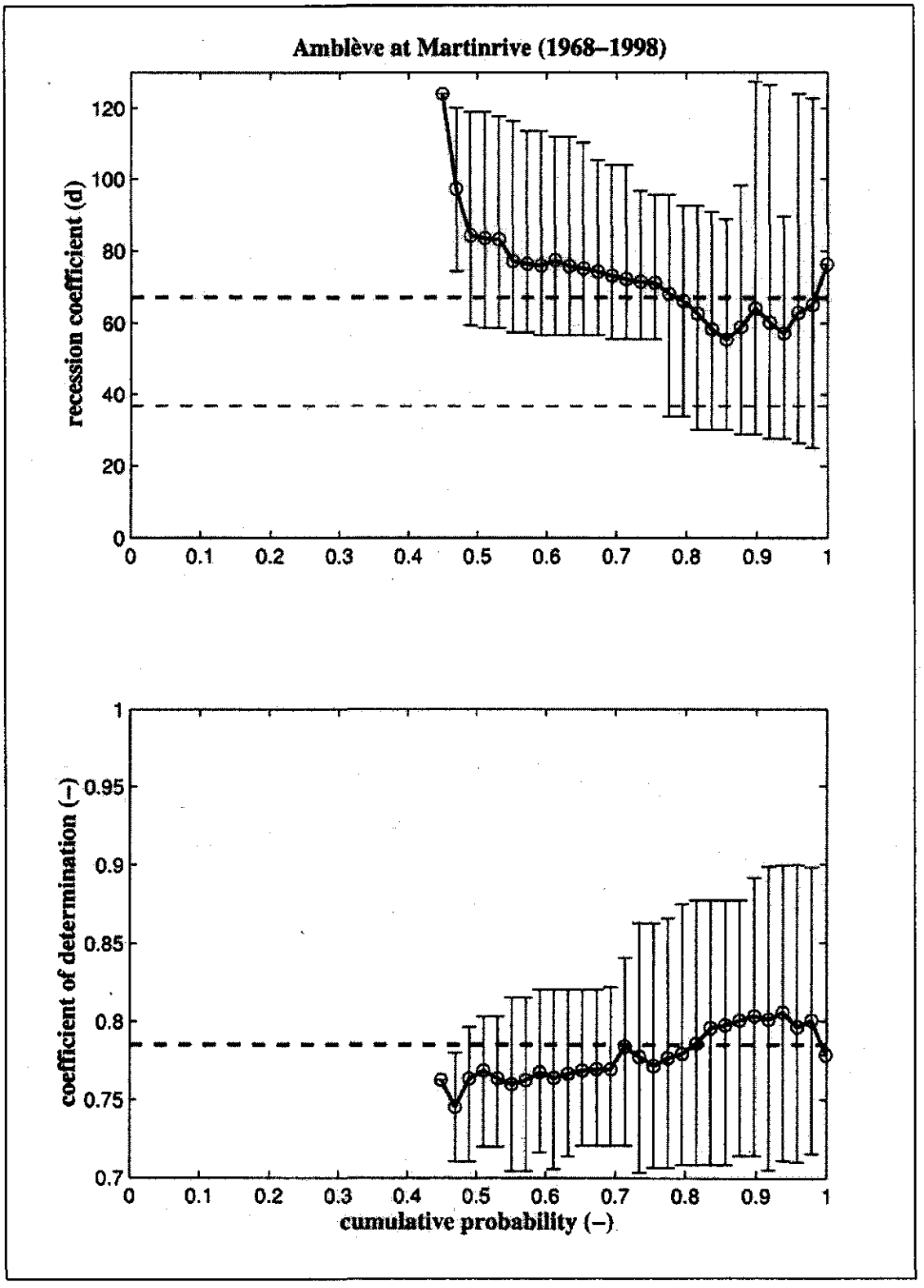

Table 8. Principal level crossing and recession characteristics of the analysed discharge time series.

#	Mean annual number of crossings (-)	Mean dry spell length (d)	Mean wet spell length (d)	Mean recession coefficient (d)	Coefficient of determination (-)
1	13.7	5.32	47.6	67.2	0.785
2	8.00	9.18	81.2	78.7	0.811
3	9.46	7.75	68.2	54.1	0.794
4	12.7	5.86	51.5	79.9	0.783
5	5.07	14.5	126	244	0.846
6	5.61	13.0	116	60.4	0.844
7	8.86	8.25	73.6	125	0.787
8	19.5	3.85	33.5	50.7	0.766
9	12.4	5.89	52.7	102	0.814
10	4.80	15.3	131	55.6	0.838
11	7.77	9.50	83.3	39.4	0.837
12	14.5	5.07	44.5	76.6	0.823
13	6.50	11.3	98.6	70.6	0.859
14	9.67	7.57	66.8	97.7	0.866
15	6.18	11.9	103	63.4	0.806
16	7.57	9.66	86.0	193	0.832
17	8.27	10.8	76.4	36.9	0.816
18	10.5	6.95	61.8	60.4	0.827
19	6.13	11.9	106	60.4	0.822
20	7.68	9.55	84.4	66.2	0.826
21	8.42	8.69	77.1	62.7	0.827
22	12.1	6.46	53.4	65.2	0.797
23	11.9	6.16	55.1	91.6	0.789

6. Intercomparison of Sub-catchments

In this chapter, the most relevant results of the previous chapters will be compared to each other and to a parameter that physically characterizes the sub-catchments: their upstream drainage areas. Figure 13 shows that both the daily mean discharge, its standard deviation, and the annual minimum and maximum discharges are very closely linearly related to the upstream drainage areas of the corresponding catchments. Table 9 quantifies these observations.

Table 9. Results of linear regression analyses of logarithmic values of mean discharges (m^3s^{-1}) and upstream drainage areas (km^2): prefactors and exponents of power law relationships, including coefficients of determination (-) and factors of proportionality.

	Prefactor of power law relationship	Exponent of power law relationship	Coefficient of determination (-)	Factor of proportionality
Mean daily discharge vs. upstream area	1.22×10^{-2}	1.01	0.973	1.24×10^{-2}
Standard deviation vs. upstream area	1.30×10^{-2}	1.02	0.938	1.42×10^{-2}
Mean annual minimum discharge vs. upstream area	3.00×10^{-3}	0.89	0.737	1.30×10^{-3}
Mean annual maximum discharge vs. upstream area	1.17×10^{-1}	0.97	0.905	7.94×10^{-2}
Mean daily discharge vs. standard deviation	1.13	1.02	0.972	1.14 (1.22)

For instance, a linear regression analysis of the logarithms of the mean daily discharges at each of the 23 gauging stations (m^3s^{-1}) versus the corresponding upstream drainage areas (km^2) confirms that these variables are very nearly linearly related. The prefactor of the resulting power law relationship is 1.22×10^{-2} and the corresponding exponent is 1.01, i.e. very close to unity (see the dashed line in the top left panel of figure 13). The coefficient of determination, a measure for the goodness-of-fit of the regression line, is 0.973, indicating a very good fit where all points more or less follow the same straight line.

Simply taking the ratio of the arithmetic mean of all mean daily discharges and the corresponding upstream drainage areas (see the dash-dotted line in the top left panel of figure 13) leads to a factor of proportionality equal to 1.24×10^{-2} $m^3km^{-2}s^{-1}$. This corresponds to 4.46×10^{-2} mmh^{-1}, since the change of units simply corresponds to multiplying by a factor 3.6. This is very close to the prefactor of the previously identified power law, again confirming the almost linearity of the relationship. The factor of proportionality may be interpreted as a characteristic specific discharge (or runoff coefficient) for the Meuse basin, somehow related to the mean annual rainfall over the catchment, its land use, soil types, topography, geology, etc. As can be seen in Table 9, the other mean discharges are also roughly linearly related to the corresponding

upstream drainage areas, although the relationships are not as close as for the mean daily discharge.

Figure 14 shows that the various measures of the speed of the discharge fluctuations bare little or no dependence on the upstream drainage areas. Figure 15 shows that the same lack of dependence holds *between* those measures. Of course, the linear relationship between the mean daily discharges and the corresponding standard deviations follows directly from Fig. 13 (top panel). This is confirmed by the numerical results presented in Table 9. Note that the ratio of the arithmetic mean of the mean daily discharges and the arithmetic mean of the corresponding standard deviations, with a value of 1.14 (dimensionless), can be interpreted as a sort of mean coefficient of variation. The actual mean coefficient of variation determined from the values for the individual gauging stations given in Table 2 is 1.22 (as indicated between brackets in Table 9).

Based on the calculated values of the statistical measures for the magnitude and speed of fluctuations (see previous chapters), the sub-catchments were ordered from 'small and slow' discharge fluctuations to 'large and fast' discharge fluctuations. This ordering was done 'by eye' and the sequence is shown in table 10. This table also gives a rough geological characterisation of the sub-catchments. This rough characterisation has been derived from BRGM (1996) and De Roeck and Tilmont (1963). It appears that some of the differences in the discharge characteristics can be explained by lithological/geological characteristics.

The sub-catchments with small and slow discharge fluctuations are those catchments that mainly consist of calcareous rocks (catchments 5, 16, 7, 9, 12, 14). One would also expect a relatively small and slow discharge fluctuation for catchments in the pleistocene sands (4 and 17). The relatively fast and large response of the catchment of the Nieuwe Leij, most probably has to be related to characteristics other than lithology. Striking is also the large and fast fluctuations in the catchments located in the Lias formation (11, 10, 15, 22). Based on the rough lithological and geological characterisation presented in table 9, one can not distinguish between the different sub-catchments in the Ardennes Massifs.

Besides lithology and basin size there are many other characteristics that influence the discharge patterns, e.g. vegetation, relief, and human interference in the form of dams, weirs and/or sluices. A complete analysis of these characteristics and their influence on the discharge is beyond the scope of the analysis presented here.

Figure 13. Scatterplots of daily mean discharge (top left panel), corresponding standard deviation (top right panel), mean annual maximum discharge (bottom left panel), and mean annual minimum discharge (bottom right panel) versus upstream drainage area for 23 gauging stations in Meuse catchment. Dashed lines indicate linear regressions of logarithm of value (dependent variable) versus logarithm of upstream drainage area (independent variable). Dash-dotted lines indicate simple proportionality between mean value and mean upstream drainage area.

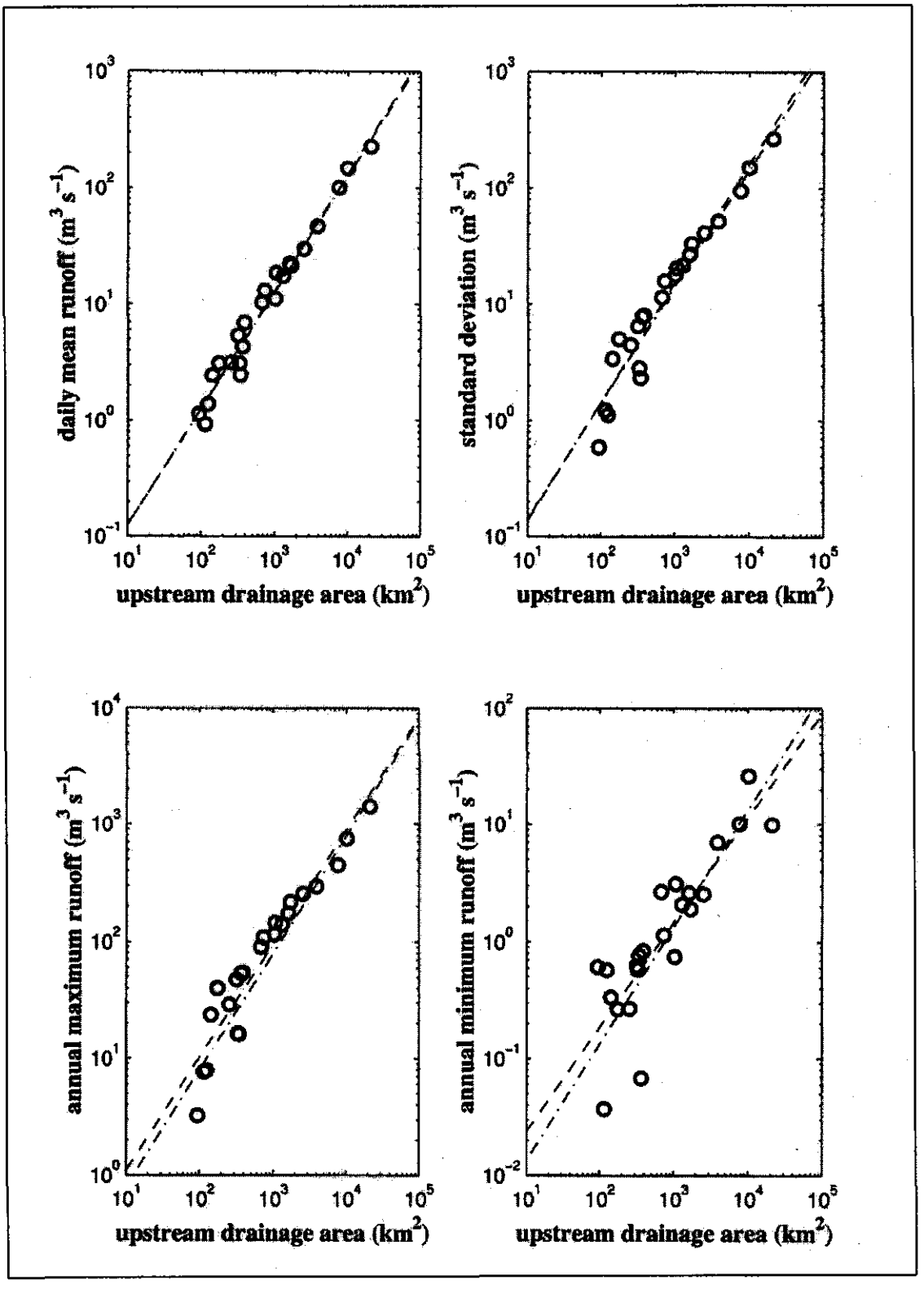

Figure 14. Scatterplots of first order autocorrelation coefficient (top left panel), scale of fluctuation of periodicity-corrected data (top right panel), mean length of dry spell associated with 10th percentile of daily discharges (bottom left panel), and mean recession coefficient (bottom right panel) versus upstream drainage area for 23 gauging stations in Meuse catchment.

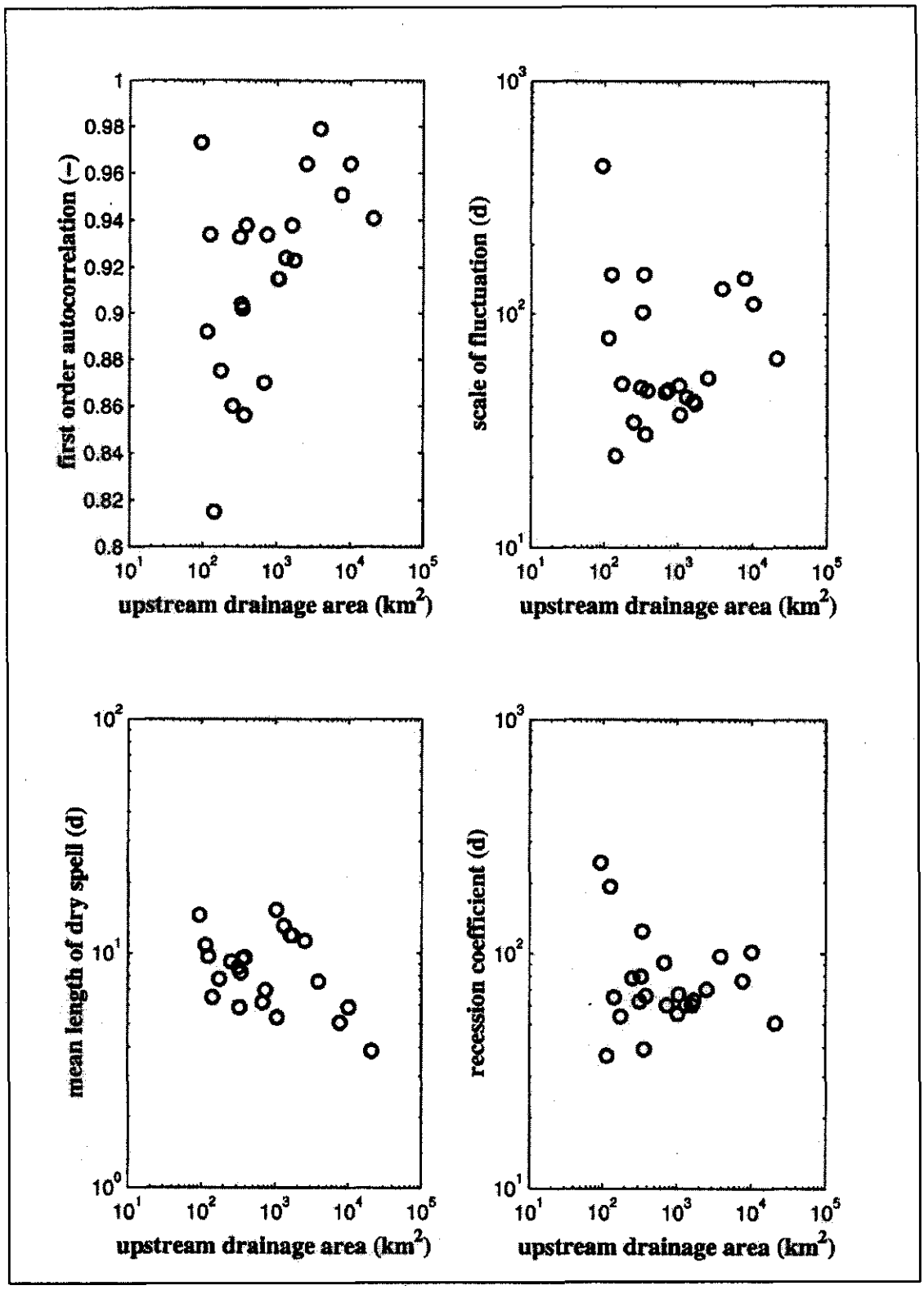

Figure 15. Scatterplots of variables from previous two figures versus each other for 23 gauging stations in Meuse catchment. In top left panel, dashed line indicates linear regression of logarithm of standard deviation of daily discharge (dependent variable) versus logarithm of mean daily discharge (independent variable) and dash-dotted lines indicate simple proportionality between mean standard deviation and mean daily discharge.

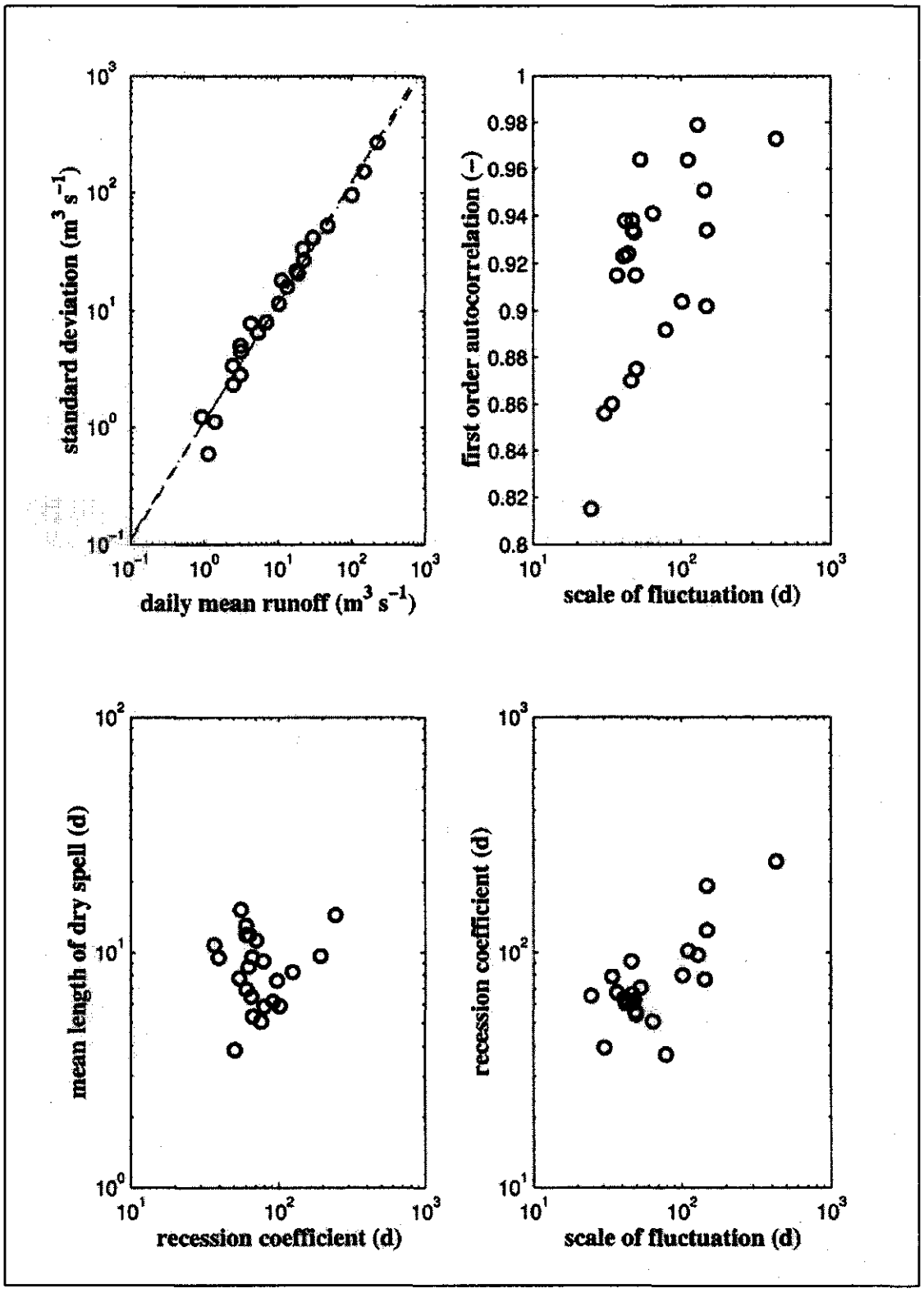

Table 10.
Rough characterisation of discharge fluctuation, lithology and geology of the 23 sub-catchments

#	River	Gauging station	Lithology	Geology
		relatively small and slow discharge fluctuations		
5	Hoyoux	Modave (B)	Limestone	Carboniferous
16	Molignée	Warnant (B)	Limestone	Carboniferous
7	Mehaigne	Moha (B)	Limestone, Sands	Tertiair, Cretaceous
4	Essche Stroom	Nemelaer (NL)	Sands	Pleistocene
9	Meuse	Chooz (F)	Limestone, Siltstone	Malm, Dogger
12	Meuse	Montcy-Notre-Dame (F)	Limestone, Siltstone	Malm, Dogger
14	Meuse	Stenay (F)	Limestone, Siltstone	Malm, Dogger
23	Vesdre	Chaudfontaine (B)	Phylitte, Quartzite, Limestone	Carboniferous, Devonian, Cambrian
1	Amblève	Martinrive (B)	Quartzite, Phylitte	Cambrian, Devonian
20	Ourthe Occidentale	Ortho (B)	Quartzite, Phylitte	Devonian
8	Meuse	Borgharen (NL)	Mixture	Mesozoic and Paleozoic
21	Ourthe Orientale	Mabompré (B)	Quartzite, Phylitte	Devonian
19	Ourthe	Tabreux (B)	Quartzite, Phylitte, Schists, Limestones	Devonian
18	Ourthe	Nisramont (B)	Quartzite, Phylitte	Devonian
6	Lesse	Gendron (B)	Quartzite, Phylitte, Shales, Limestones	Devonian
17	Nieuwe Leij	Goirle (NL)	Sands	Pleistocene
13	Meuse	Saint-Mihiel (F)	Limestone, Siltstone, Sandstone	Malm, Dogger, Lias
22	Semois	Ste. Marie (B)	Sandstone, Siltstone	Lias, Trias
2	Eau Blanche	Nismes (B)	Quartzite, Phylitte, Shales, Limestone	Devonian
15	Meuse	Vaucouleurs / Chalaines (F)	Limestone, Siltstone and Sandstone	Dogger, Lias
10	Meuse	Domrémy-la-Pucelle (F)	Sandstone, Siltstone, Limestone	Dogger, Lias
3	Eau Noire	Couvin (B)	Quartzite, Phylitte	Devonian, Cambrium
11	Meuse	Goncourt (F)	Sandstone, Siltstone	Lias
		relatively large and fast discharge fluctuations		

7. Recommendations

Below some recommendations are given to improve and extend the analyses presented in this report:

- Look in more detail to the relations between discharge characteristics and catchment characteristics such as lithology, vegetation, topology, soils, and human interference;
- Calculate the recession coefficients and other statistics separately for the summer and for the winter half year;
- Compare the proposed automated method for calculating recession coefficients with results of other approaches presented in the literature (e.g. Berger, 1992);
- Extend the definition of recession coefficients to include power law recession behaviour (e.g. Troch *et al.*, 1993);
- Look in more detail at the (spatial) correlation structure of discharges between gauging stations;
- Extend the results obtained in this report to include precipitation and evaporation data.

References

Berger, H.E.J. (1992). *Flow forecasting for the river Meuse*. PhD Thesis, Delft University of Technology, The Netherlands, 356 p.

BRGM (1996). Carte Geologique de la France à 1/1 000 000. Orléans, France.

De Roeck, M. and Tilmont, J. (1963). General Atlas Belgium. Wesmael-Charlier, Namur, Belgium.

Gellens, D. and E. Roulin (1998). Streamflow response of Belgian catchments to IPCC climate change scenarios. *Journal of Hydrology* **210**, 242-258.

Gellens, D., E. Roulin, and F. Gellens-Meulenberghs (1998). Impact of climate change on the water balance in the river Meuse basin (Belgium). Results obtained by moving scale from 200 to 2000 km^2. In: *Proceedings of the 2nd International Conference on Climate and Water*, Espoo, Finland, 17-20 August 1998, 820-828.

Haan, C.T. (1977). *Statistical methods in hydrology*. The Iowa State University Press, Ames, 378 p.

Kendall, M.G. and A. Stuart (1977). *The advanced theory of statistics, Volume I: Distribution theory*. Charles Griffin, London, 472 p.

Sen, Z. (1980). Statistical analysis of hydrologic critical droughts. *ASCE Journal of the Hydraulics Division* **106**, 99-115.

Troch, P.A., F.P. De Troch, and W. Brutsaert (1993). Effective water table depth to describe initial conditions prior to storm rainfall in humid regions. *Water Resources Research* **29**, 427-434.

Van Deursen, W.P.A. (1999). *MEUSEFLOW: An integrated GIS water balance model for the river Meuse*. RIZA Report X.

VanMarcke, E. (1983). Random fields: analysis and synthesis. The MIT Press, Cambridge, 382 p.

Appendices (on CD)

1 Figure 1

Representation of 'raw' data analysed in this report: entire mean daily discharge time series for all 23 gauging stations in Meuse catchment.

2 Figure 2

Mean yearly discharge time series (top panel), 2-year aggregation (middle panel), and 5-year aggregation (bottom panel) for 23 gauging stations in Meuse catchment, including 10/90 (thin error bars) and 25/75 percentiles (bold error bars).

3 Figure 3

Mean daily discharge throughout calendar year (top panel) and 10-day aggregation (bottom panel) for 23 gauging stations in Meuse catchment, including 10/90 (both, thin error bars) and 25/75 percentiles (only 10-day aggregations, bold error bars).

4 Figure 4

Three different representations of cumulative distribution of daily discharges for 23 gauging stations in Meuse catchment: direct (top panel), on exponential probability paper (middle panel), and on lognormal probability paper (bottom panel). Dashed line indicates mean daily discharge.

5 Figure 5

Plots of annual minimum series (circles) and partial duration series (plusses) of (non-zero) daily discharges for 23 gauging stations in Meuse catchment on lognormal (top panel) and Weibull (bottom panel) probability paper. Dashed lines indicate linear regression of logarithm of minimum daily mean discharge (dependent variable) versus standard normal and standard Weibull variates (independent variables).

6 Figure 6

Plots of annual maximum series (circles) and partial duration series (plusses) of daily discharges for 23 gauging stations in Meuse catchment on lognormal (top panel) and Gumbel (bottom panel) probability paper. Dashed lines indicate linear regression of (logarithm of) maximum daily mean discharge (dependent variable) versus standard normal and standard Gumbel variates (independent variables).

7 Figure 7

Empirical autocorrelation function (direct, top panel, and semi-logarithmically, middle panel) and two-sided spectral density function (bottom panel) of daily discharges for 23 gauging stations in Meuse catchment, with (bold lines) and without (thin lines) correction for seasonal periodicity in mean and standard deviation. In top two panels, dashed horizontal lines indicate regions where autocorrelation significantly (with 99% confidence) departs from zero and dash-dotted vertical lines indicate scale of fluctuation of periodicity-corrected data. In bottom panel, crosses indicate spectral densities at zero frequency, circle indicates scale of fluctuation of periodicity-corrected data, and vertical lines indicate frequencies of once per week (solid), once per month (dashed), and once per year (dash-dotted).

8 Figure 8

Mean annual number of crossings (top panel), mean (solid line) and standard deviation (dashed line) of lengths of dry spells (middle panel), and mean (solid line) and standard deviation (dashed line) of lengths of wet spells (bottom panel) associated with 50 quantiles of daily discharge (linearly spaced between 0.001 and 0.999) for 23 gauging stations in Meuse catchment. In bottom two panels, error bars indicate values of minimum and maximum length of dry and wet spells at given quantile.

9 Figure 9

Three different representations of cumulative distribution of lengths of dry spells associated with 10th percentile of daily discharges for 23 gauging stations in Meuse catchment: direct (top panel), on exponential probability paper (middle panel), and on lognormal probability paper (bottom panel). Dashed lines indicate mean length of dry spell at given quantile.

10 Figure 10

Three different representations of cumulative distribution of lengths of wet spells associated with 10th percentile of daily discharges for 23 gauging stations in Meuse catchment: direct (top panel), on exponential probability paper (middle panel), and on lognormal probability paper (bottom panel). Dashed lines indicate mean length of wet spell at given quantile.

11 Figure 11

First order autocorrelation coefficients of subsequent dry spells (top panel), wet spells (middle panel) and dry and wet spells (bottom panel) associated with given quantiles of daily discharges for 23 gauging stations in Meuse catchment. Dashed lines indicate regions where autocorrelation significantly (with 99% confidence) departs from zero.

12 Figure 12

Recession coefficients (top panel, circles / bold solid line) and corresponding coefficients of determination (bottom panel, circles / bold solid line) associated with given quantiles of daily discharges for 23 gauging stations in Meuse catchment. Error bars indicate minimum and maximum values at given quantile and bold dashed lines indicate mean values over all quantiles. Thin dashed line in top panel indicates scale of fluctuation of periodicity-corrected data.

A Program ReadData

Reading names of rivers and towns corresponding to 23 discharge measurement stations in Meuse catchment, associated upstream drainage areas (km2) and first and last years of longest uninterrupted discharge time series (in entire calendar years) from datafile into variables

B Program MaasFile

Merging individual discharge datafiles for 23 stations in French, Belgian and Dutch part of Meuse catchment into single datafile; resulting file consists of 23 columns corresponding to 23 rivers in alphabetical order - see file "STATIONS.TXT") and 11323 rows (corresponding to all days from 1 January 1968 to 31 December 1998); data for each station correspond to longest uninterrupted discharge time series (in entire calendar years), with remaining data flagged using "ErrorFlag"; numbers in resulting datafile represent mean daily discharges in m3/s

C Program MaasFlo01

Creating postscript figure(s) with mean daily discharge time series for 23 measurement stations in Meuse catchment (3 years on 1 page)

D Program MaasFlo02

Creating postscript figure(s) with mean yearly discharge time series, 2-year aggregations, and 5-year aggregations for 23 measurement stations in Meuse catchment, including 10/90 and 25/75 percentiles

E Program MaasFlo03

Creating postscript figure(s) with mean daily discharge throughout calendar year and 10-day aggregations for 23 measurement stations in Meuse catchment, including 10/90 (both) and 25/75 percentiles (only 10-day aggregations)

F Program MaasFlo04

Creating postscript figure(s) with 3 different representations of cumulative distributions of daily discharges for 23 measurement stations in Meuse catchment: direct, on exponential probability paper, and on lognormal probability paper; calculating total number of days and number of days with zero discharge in each time series; calculating 10 statistics of (non-zero) daily discharges: mean (m3/s), standard deviation (m3/s), coefficient of variation (-), coefficient of skewness (-), coefficient of kurtosis (-), minimum (m3/s), 10th percentile (m3/s), median (m3/s), 90th percentile (m3/s), and maximum (m3/s)

G Program MaasFlo05

Creating postscript figure(s) with plots of both annual minimum series and partial duration series of (non-zero) daily discharges for 23 measurement stations in Meuse catchment on lognormal and Weibull probability paper; calculating 4 statistics of annual minimum series: mean (m3/s), standard deviation (m3/s), and coefficients of determination of lognormal and Weibull fits (-)

H Program MaasFlo06

Creating postscript figure(s) with plots of both annual maximum series and partial duration series of daily discharges for 23 measurement stations in Meuse catchment on lognormal and Gumbel probability paper; calculating 4 statistics of annual maximum series: mean (m3/s), standard deviation (m3/s), and coefficients of determination of lognormal and Gumbel fits (-)

I Program MaasFlo07

Creating postscript figure(s) with autocorrelation functions (direct and semi-logarithmic plots) and 2-sided spectral density functions of daily discharges for 23 measurement stations in Meuse catchment, with and without correction for seasonal periodicity in mean and standard deviation; calculating 3 statistics of (un)corrected autocorrelation function / spectrum: first order autocorrelation coefficient (-), decorrelation time (d), and scale of fluctuation (d)

J Program MaasFlo08

Creating postscript figure(s) with 3 different representations of cumulative distributions of lengths of dry and wet spells for given quantile of daily discharges for 23 measurement stations in Meuse catchment: direct, on exponential probability paper, and on lognormal probability paper; calculating corresponding mean annual number of crossings (-) and mean lengths of dry and wet spells (d)

K Program MaasFlo09

Creating postscript figure(s) with numbers of crossings (-), means and standard deviations of lengths of dry spells (d), means and standard deviations of lengths of wet spells (d), first order autocorrelation coefficients of subsequent dry and wet spells (-), recession coefficients (d), and corresponding coefficients of determination (-) for given quantiles of daily discharges for 23 measurement stations in Meuse catchment; calculating mean recession coefficients (d) and corresponding mean coefficients of determination (-) for individual daily discharge time series

L Program MaasFlo10

Creating postscript figure(s) with scatterplots of daily mean discharge (m3/s), corresponding standard deviation (m3/s), mean annual maximum and minimum discharge (m3/s), first order autocorrelation coefficient (-), scale of fluctuation (d), mean length of dry spell for given discharge quantile (d), and mean recession coefficient (d), both versus upstream drainage area (km2) and versus each other, for 23 measurement stations in Meuse catchment